Defining the heterogeneous molecular landscape of lung cancer cell responses to epigenetic inhibition

Authors

Chuwei Lin[1], Catherine M. Sniezek[1], Christopher D. McGann[1], Rashmi Karki[2], Ross M. Giglio[3], Benjamin A. Garcia[2], José L. McFaline-Figeroa[3], Devin K. Schweppe[1,4,5], *

1 Genome Sciences, University of Washington, Seattle, WA 98105, USA

2 Department of Biochemistry and Molecular Biophysics, Washington University School of Medicine, St. Louis, MO 63110, USA

3 Biomedical Engineer, Columbia University, New York, NY 10027, USA

4 Brotman Baty Institute for Precision Medicine, Seattle, Washington, USA

5 Institute of Stem Cell and Regenerative Medicine, University of Washington, Seattle, Washington, USA

*Email: dkschwep@uw.edu

Summary

Epigenetic inhibitors exhibit powerful antiproliferative and anticancer activities. However, cellular responses to small-molecule epigenetic inhibition are heterogenous and dependent on factors such as the genetic background, metabolic state, and on-/off-target engagement of individual small-molecule compounds. The molecular study of the extent of this heterogeneity often measures changes in a single cell line or using a small number of compounds. To more comprehensively profile the effects of small-molecule perturbations and their influence on these heterogeneous cellular responses, we present a molecular resource based on the quantification of chromatin, proteome, and transcriptome remodeling due to histone deacetylase inhibitors (HDACi) in non-isogenic cell lines. Through quantitative molecular profiling of 10,621 proteins, these data reveal coordinated molecular remodeling of HDACi treated cancer cells. HDACi-regulated proteins differ greatly across cell lines with consistent (JUN, MAP2K3, CDKN1A) and divergent (CCND3, ASF1B, BRD7) cell-state effectors. Together these data provide valuable insight into cell-type driven and heterogeneous responses that must be taken into consideration when monitoring molecular perturbations in culture models

Introduction

Deconvoluting the myriad effects downstream of small molecule perturbations is essential to therapeutic development. Whole proteome and transcriptome analyses of these perturbations can validate and identify proposed mechanisms of action and identify cellular effects for therapeutics and tool compounds. To date, however, many of the large-scale proteome analyses of drug perturbations have been either limited to one or a few cell lines treated with a cohort of small-molecule tool compounds and therapeutic drugs (Supplementary table 1). The use of these sets of cell lines has been in part a practical consideration owing to the rapid expansion of samples that must be processed and compared with each individual drug treatment. Unfortunately, this often means sacrificing understanding of the diverse molecular contexts of different cellular models to enable the analysis of larger cohorts of small-molecule compounds (P.-H. Chen et al., 2019).

Large-scale viability screening of small molecule perturbations in the PRISM dataset has shown that drugs targeting the same protein or pathway can drive heterogeneous responses in cancer cells (Corsello et al., 2020). Recent transcriptome efforts for bulk and single-cell samples have uncovered some of the molecular disparity in cellular responses when cells are treated with therapeutic and tool compounds

(Srivatsan et al., 2020). At the single-cell level, these studies revealed inconsistent molecular responses of individual, isogenic cells to small molecule perturbation suggesting that additional context and molecular understanding are necessary to dissect the molecular consequences of chemical perturbation. In particular, transcriptomic profiling of cellular perturbations cannot fully explain proteomic consequences in cells (Maltz & Wollman, 2022). Owing to the limited correlation between RNA and protein measurements (D. Wang et al., 2019), there remains a gap in our knowledge of the proteomic consequences of drug perturbations across multiple, representative cell lines.

Recently, several studies have aimed to bridge this gap. These include the DeepCoverMOA and decryptE datasets (Mitchell et al., 2023; Zecha et al., 2023), which represent some of the largest, publicly-available chemical perturbation-based proteomic datasets. The DeepCoverMOA analyzed HCT116 cells in response to 875 therapeutic and tool compounds and revealed that a majority of the measurable proteome was accessible to regulation by small molecule treatment. The resulting proteome remodeling responses were then used to assemble proteomic networks to define consistent chemical mechanisms of actions. In a related study, the decryptE dataset studied dose-dependent chemical responses of 144 compounds in Jurkat cells to determine similarities and differences in cellular mechanisms of action. Yet, an important caveat to these two studies was that the whole proteome analysis to decipher compound mechanisms of action were each done in single, isogenic cell lines which may not be representative of the genetic and molecular heterogeneity when considering non-isogenic cell models (Begley & Ellis, 2012; Raghavan, 2022). Interestingly, both the DeepCoverMOA and decryptE datasets evidenced high overall compound activity for histone deacetylase (HDAC) inhibitors (HDACi) such as vorinostat, quisinostat, and nexturastat (Mitchell et al., 2023; Zecha et al., 2023).

HDAC regulation is key to the cellular chromatin state and is frequently dysregulated in cancer (Y. Li & Seto, 2016) and known to exhibit lineage-specific dependencies in cancer cells (Y. Zhang et al., 2023). This relationship between HDACs and cancer progression has driven a decades-long effort to develop targeted chemical HDAC inhibitors (HDACi) (Yoshida et al., 1990) and FDA approvals for several of these inhibitors to treat lymphomas and melanomas (B. S. Mann et al., 2007; McDermott & Jimeno, 2014; Richardson et al., 2015). While HDAC inhibitors have shown promising preclinical results for many cancers, clinical trial results vary (Mamdani & Jalal, 2020). Vorinostat monotherapy in non-small cell lung cancer (NSCLC) patients did not show objective antitumor activity, but toxicity with adverse effects such as fatigue (Traynor et al., 2009). Other phase II monotherapy of romidepsin and pivaloyloxymethyl butyrate resulted in little efficacy in patients, and had side effects such as fatigue, nausea, and dysgeusia (Reid et al., 2004; Schrump et al., 2008). While comprehensive understanding of the pleiotropic molecular consequences remains elusive (Miyanaga et al., 2008), treatment of cells with HDACi induces expression of p21/CDKN1a leading to cell cycle arrest (Richon et al., 1996) (Xiao et al., 1999), alters expression of c-Jun (Vrana et al., 1999) and the apoptotic regulators Bcl-2 and Bcl-xL (X. X. Cao et al., 2001; Fandy & Srivastava, 2006), attenuates AKT/mTOR signaling leading to autophagy (Y.-L. Liu et al., 2010), and suppresses IFN-mediated signaling (Shulak et al., 2014). Recent chemoproteomics analyses have also revealed that heterogeneous responses to HDAC inhibition may be driven in part by the abundance of HDAC protein complex members and the engagement of off-target HDACi binders such as MBLAC2 (Lechner et al., 2022). Thus, these effects have been shown to be both cell-type dependent and cell-type independent, further confounding our understanding of the molecular consequences of HDACi cellular treatments.

Here, we set out to determine the effects of the HDACi treatment on proteome remodeling in non-isogenic cell lines. In particular we focused on cell treatments with well established HDACi compounds to enable comparative analyses to previous datasets such as DeepCoverMOA and decryptE—including, belinostat, CUDC-101, trichostatin A (TSA), panobinostat, abexinostat and vorinostat (SAHA). We did this in the context of a genetically diverse panel of lung cancer cell lines with KRas, EGFR, TP53, CDKN1A, STK11 mutations and integrated proteomic, phosphoproteomic, and transcriptomics to

establish a resource to explore drivers of the heterogeneous HDACi responses in these cells. Quantification of histone modifications status in multiple cell lines and thermal stability analyses then allowed us to determine the molecular linkage and effects of on-target and off-target protein engagement with HDAC inhibitors. These data represent an important resource to understand how chemical perturbation analyses are affected by preclinical cell line choice and exploration of how cellular diversity affects the characterization of small molecule compound mechanisms of action.

Result

Heterogeneous responses of cancer cells treated with epigenetic inhibitors

Proteomic studies of the responses of cells to small-molecule drug perturbations have been a powerful means to understand diverse mechanisms of action for therapeutic and tool compounds (Eckert et al., 2024; Mitchell et al., 2023; Zecha et al., 2023). Yet, these studies often rely on single, isogenic cell lines to characterize chemical perturbation effects. To understand how cancer cell lines with non-isogenic backgrounds respond to pleiotropic effects of drug perturbations we sought to measure proteomic remodeling of multiple lung cancer cell lines with diverse, and representative, genetic backgrounds in the context of lung cancer—e.g., KRas, EGFR, TP53, CDKN1A, STK11 mutations. Based on the strength of proteome remodeling previously reported in proteomic (decryptE and DeepCoverMOA) and transcriptomic (Sci-plex) datasets (Mitchell et al., 2023; Srivatsan et al., 2020; Zecha et al., 2023), we focused on perturbations driven by HDAC inhibition (Eckert et al., 2024; Zecha et al., 2023). We selected six established HDAC inhibitors with known canonical and off-target effects, including belinostat (pan-HDACi), CUDC-101 (pan-HDACi, HER2/EGFR inhibitor) (Y. Li & Seto, 2016; Shanmugam et al., 2022), trichostatin A (TSA, pan-HDACi), panobinostat, abexinostat (HDAC1/2/3/6/8/10 inhibitor)(Buggy et al., 2006), and vorinostat (pan-HDACi). To ensure that we could robustly capture proteome remodeling effects at the cell-type- and compound-specific level, we also treated these cell lines with the p38 kinase inhibitor ralimetinib as an outgroup.

We then chose five representative cancer cell models to measure the effects of HDACi perturbations—HCT116, A549, PC9, H292, and PSC1 cells. We included HCT116 colon cancer cells and A549 lung cancer cells (adenocarcinoma line with KRAS mutation) as they have both been characterized in proteomic (Mitchell et al., 2023; Nusinow et al., 2020) and transcriptomic (Srivatsan et al., 2020; Tsherniak et al., 2017) chemical perturbation analyses. We then focused on NSCLC cell lines for the other three cell lines as this cancer subtype was known to present divergent preclinical and clinical responses to HDACi treatments (Mamdani & Jalal, 2020). These three additional cell lines were chosen for their divergent mutational statuses, with a focus on lung cancer cells lines: H292 is a mucoepidermoid carcinoma line (CRTC1-MAML2 fusion, NF2 P496Tfs), PC9 is an adenocarcinoma line (EGFR E746_A750del, TP53 R248Q), and PSC1 is a doxorubicin-resistant derivative of the INER-51 adenocarcinoma cell line (P-gp/MDR-1 negative; Supplementary table 2). We selected these cells in part based on their drug responses in the PRISM drug repurposing screen (Tsherniak et al., 2017). Of our five cell lines, four overlapped with the PRISM screen (A549, PC9, A549, HCT116) and the mean responses of these four cell lines together performed better at recapitulating average drug responses for all 1,941 cancer cell lines in the PRISM dataset than any single cell line (four cell lines: $r_{pearson} = 0.836$; PC9: $r_{pearson} = 0.706$; HCT116: $r_{pearson} = 0.702$; H292: $r_{pearson} = 0.625$; A549: $r_{pearson} = 0.593$, Figure 1A).

To assess whether HDACi compounds would drive divergent cellular responses in our cell line cohort, we first compared the effects of treatment on cellular viability in each of the five cell lines treated with each of the HDACi compounds (Figure 1B). We chose the concentration and perturbation timing to be consistent with, and enable comparison to, previous proteomic and transcriptomic datasets (Supplementary table 1)(Corsello et al., 2020; Eckert et al., 2024; Mitchell et al., 2023; Srivatsan et al., 2020; Zecha et al., 2023), thus, cells were incubated with 10 µM of each compound or vehicle control (DMSO) for 24 hours prior to viability assays (Figure 1B). As expected, each of the cell lines was

differentially sensitive toward the seven tested compounds (Figure 1C). PC9 cells were highly sensitive to HDACi and ralimetinib treatment, especially CUDC-101 (Figure 1C). The sensitivity to CUDC-101 may be driven by the known off-target inhibition of EGFR by CUCD-101 as PC9 cells harbor a gene amplification of EGFR (Nukaga et al., 2017) and these cells are known to be sensitive to EGFR inhibition with 10μM gefitinib (Nukaga et al., 2017). Additionally, A549 cells were sensitive to belinostat to a greater extent than any of the other HDACis. Conversely, PSC1 cells were the most insensitive to HDACi and ralimetinib treatment.

Based on the divergent phenotypic responses of these cell lines to HDAC inhibition, we performed quantitative proteomic analysis of the 35 single-perturbation, cell-by-drug combinatorial treatments (10 μM of each drug or vehicle control (DMSO) for 24 hours, Supplementary Figure 1A). In total, we quantified 476,387 unique peptides, 6,615 phosphorylation sites, and 10,621 unique proteins. Protein quantification between biological replicates was highly reproducible with a median Pearson correlation (r) for biological replicates of each drug and cell line of 0.996 (Supplementary Figure 1B). The median coefficient of variation (%CV) for protein measurements between two biological replicates was 4.4% (Supplementary Figure 1C). Each cell line was quantified to an average depth of 8,125 proteins (Supplementary Figure 1D). Of the 10,621 total unique proteins, 6,145 proteins were found in all five cell lines, 8,083 proteins were found in at least three cell lines, and 1,311 were found in only one cell line (Supplementary Figure 1E).

Comparison of our data to the DeepCoverMOA (Mitchell et al., 2023) and decryptE (Eckert et al., 2024) datasets allowed us to compare the diversity and consistency of cellular responses (Figure 1D). To do this we calculated the correlation between each cell-by-drug treatment in our data and the DeepCoverMOA and decryptE datasets (Figure 1D). Proteome remodeling of HCT116 cells treated with vorinostat in our dataset were highly correlated with HCT116 cells treated with vorinostat in DeepCoverMOA ($r_{Pearson}$ = 0.86, slope = 1.01, Figure 1E). This was driven in part by known HDACi responsive proteins, such as increased abundance of cyclin-dependent kinase inhibitor 1 (CDKN1A) and cyclin-D3 (CCND3) (Richon et al., 2000; Siavoshian et al., 2000); increased abundance of transcription factor and oncoprotein c-Jun (JUN) and decreased abundance of HDAC7 (Ma & D'Mello, 2011); and reduced abundance of cyclin-A2 (CCNA2) (Majumdar et al., 2012). DeepCoverMOA vorinostat clustered together with our HCT116 cells data, but not other cells with vorinostat.

Confirming our initial speculation that the cellular context of proteome mechanism of action studies is an important consideration, proteome remodeling with vorinostat treatment in the additional cancer cell lines was less well correlated to DeepCoverMOA HCT116 cell responses. Correlation between the four lung cancer cells with vorinostat treatment and DeepCoverMOA vorinostat was quite variable even when considering cell lines with shared mutational status to HCT116 cells ($r_{Pearson}$ = 0.50-0.69, Figure 1D). A549 cells treated with vorinostat had the highest correlation with DeepCoverMOA vorinostat ($r_{Pearson}$ = 0.69), which may be because both A549 and HCT116 are KRAS and SMARCA4 mutants. PC9 cells with vorinostat had the lowest correlation compared to the DeepCoverMOA data ($r_{Pearson}$ = 0.50, Figure 1E). Anecdotally, we note that this was consistent with PC9 cells being the most sensitive to HDACi perturbations (Figure 1C). Compared to HCT116 and other lung cell lines, we found that PC9 cells did not increase the abundance of JUN in response to HDACi treatment (Figure 1E). Additionally, we compared our belinostat, TSA and vorinostat treatment data and the decryptE analysis of HDACi treatment of Jurkat cells (Eckert et al., 2024). The correlations between Jurkat cells and four lung cancer cells with belinostat, TSA and vorinostat treatment were much lower than those we observed for the HCT116 treatments in the DeepCoverMOA study ($r_{Pearson}$ = 0.15-0.50, Figure 1D). These data highlight the importance of considerations of the cellular context of cells when assessing mechanism of action and polypharmacology using proteomics.

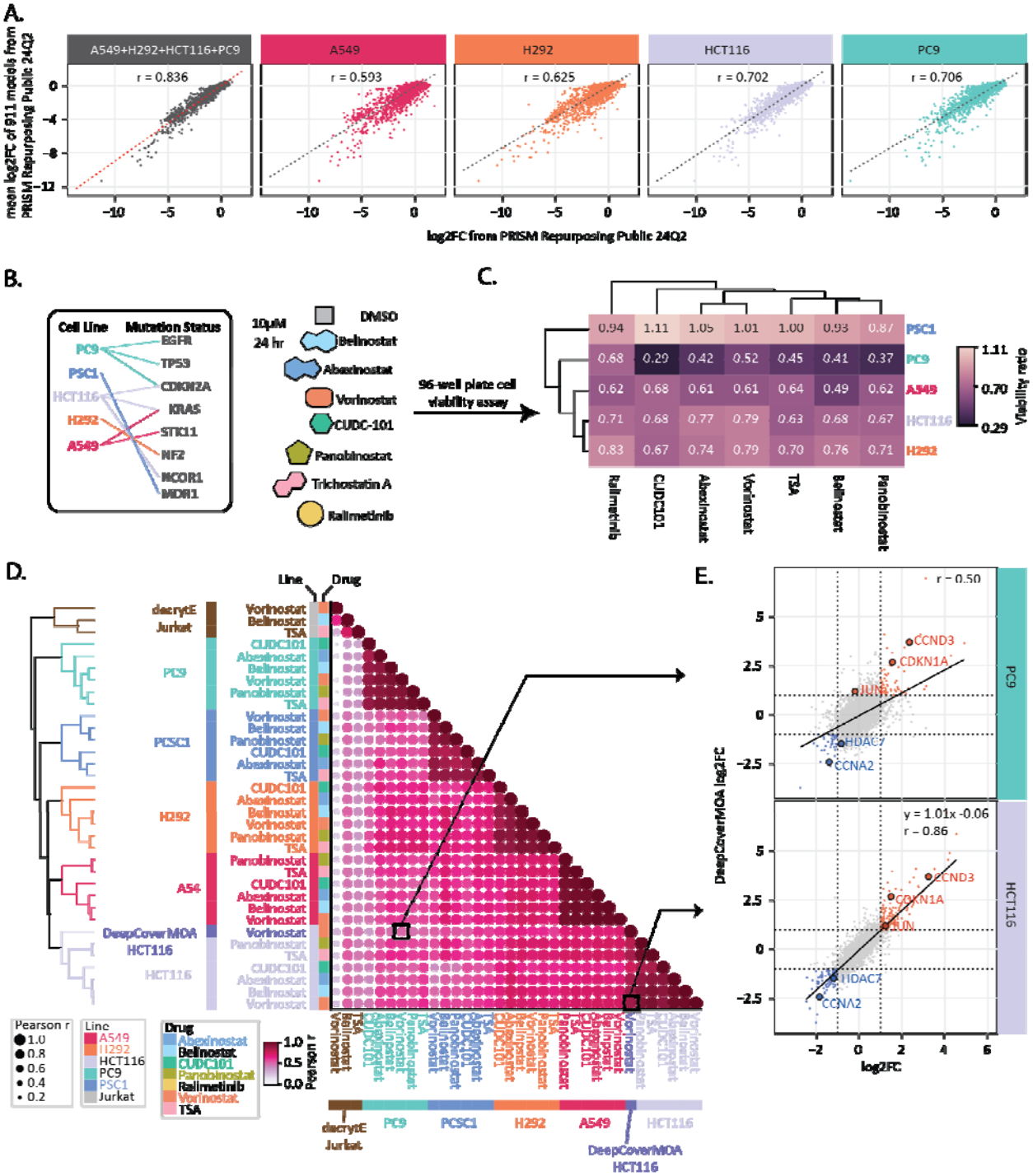

Figure 1. Heterogeneous responses in cancer cells. A, Comparison of viability of 4 cell lines, A549, H292, HCT116 and PC9, from PRISM drug repurposing public 24Q2. Each point represents one compound tested on the corresponding cell line. The x axis is log2 fold change of viability compared with negative control of each corresponding cell line. The y axis is the mean of log2 fold change of viability compared with negative control of 911 cell line models. **B,** Experimental setup of viability assay and proteomics. Five cell lines were treated with 10 uM of each compound for 24 hours. **C,** Viability of each cell line in response to 7 drugs normalized to DMSO treated controls. Viability was measured by luminescent cell viability assay. Viability ratio is drug treated cells/DMSO treated cells. **D,** Pearson

correlation analysis comparing HDACi treated samples in our dataset (10uM HDACi, 24 hours, HCT116, A549, PSC1, PC9, H292), DeepCoverMOA (10uM HDACi, 24 hours, HCT116), and decryptE (10 uM HDACi, 18 hours, Jurkat). **E**, Scatterplots highlight specific results from the correlation analysis for (top) the poorly correlated vorinostat-treated HCT116 cells from the DeepCoverMOA study compared to vorinostat-treated PC9 cells from this study and, (bottom) highly correlated vorinostat-treated HCT116 cells from the DeepCoverMOA study compared to vorinostat- treated HCT116 cells from this study. The log2FC is the protein abundance change with vorinostat treatment compared with DMSO treatment.

The landscape of proteome responses to HDACi perturbation of cancer cells

Treatment of five cell lines with seven drugs resulted in 35 cell-line-by-drug groups enabled well-powered proteome-wide co-regulation analyses ($\rho_{estimated}$~0.87). We quantified the relative abundance of proteins in comparison of vehicle (DMSO) controls for each of these perturbations and replicate analyses generated highly correlated proteome abundance shifts (Supplementary Figure 1A). The six HDACi and ralimetinib all have the potential to drive pleiotropic remodeling of proteins and protein complexes (Mader et al., 2008; Mamdani & Jalal, 2020). Interestingly, though the HDACi compounds drove strong proteome remodeling, PCA analysis generally clustered cell-line-by-drug groups based on cell lines, not the compound used to treat these cells. The one notable difference was that compared to matched vehicle controls in each cell line, ralimetinib-treated cells clustered together in principal component space irrespective of the cell line (Figure 2A).

In total, we observed 14,856 cell-line-by-drug regulated events across all groups on 2,327 different proteins (|log2FC| > 1, Supplementary Figure 2A, Supplementary data 1). Among the 2,327 regulated proteins, only 15 proteins were differentially abundant in at least 30 cell-line-by-drug groups (Figure 2B). These included the beta-catenin antagonist DACT3, the interferon induced OASL oligoadenylate synthetase, the TP63-like protein TPRG1L, and cell cycle related proteins such as MLF1, CCND3, CCN2. Several of these consistent protein responses were seen previously, such as the increased DACT3 protein abundance with TSA treatment (Jiang et al., 2008). In addition to these semi-ubiquitous HDACi-responsive proteins, we quantified 2,282 proteins that were differentially abundant in less than 14 cell-line-by-drug groups—suggesting cell type- or cell state-specific responses (Supplementary Figure 2A). The heterogeneity of proteome remodeling with drug treatment was consistent with heterogeneity in the cell line viability analysis (Figure 1A) and can offer important clues as to the differential susceptibility of these cell models to HDACi perturbation.

Based on the total number of regulated proteins, we observed the largest degree of proteome remodeling in HDACi-treated A549 cells (Figure 2C, Supplementary Figure 2B). Conversely, our outgroup treatment of cells with ralimetinib generated the lowest number of regulated proteins (Figure 2C). The chemoresistant PSC1 cells had the lowest number of regulated proteins among all tested cell lines which is consistent with the limited effect of drug treatment on cellular viability in these cells. When comparing compound-specific effects, belinostat treatment of lung cancer cells (A549, H292, PC9 and PSC1) consistently generated the largest degree of proteome remodeling, followed by panobinostat, abexinostat, TSA, CUDC-101 and vorinostat (Figure 2C, 2D).

To dissect what pathways may be playing a role in the divergent responses of cells to HDACi treatment, we performed hallmark enrichment analysis (Liberzon et al., 2015). We found that proteins with differential abundance with HDACi treatment were significantly enriched for consistent with TNF-alpha signaling via NF-kB and UV response pathways (Figure 2E, 2F). Notably, some pathways were only significantly regulated in a specific subset of cell lines. For example, mTORC1 associated proteins were only enriched in A549 and H292 cells treated with HDACi. Notably, this did not correlate with the background mutational status of these cell lines as A549 cells are driven by a constitutively-active KRas

mutant and H292 cells are driven by the loss of the NF2 tumor suppressor (van der Meer et al., 2019). Interestingly, proteins involved in p53 pathways mainly had increased abundance in A549 and HCT116 cells, while they had decreased abundance in H292 and PC9 cells, and these proteins were not differentially regulated in PSC1 cells.

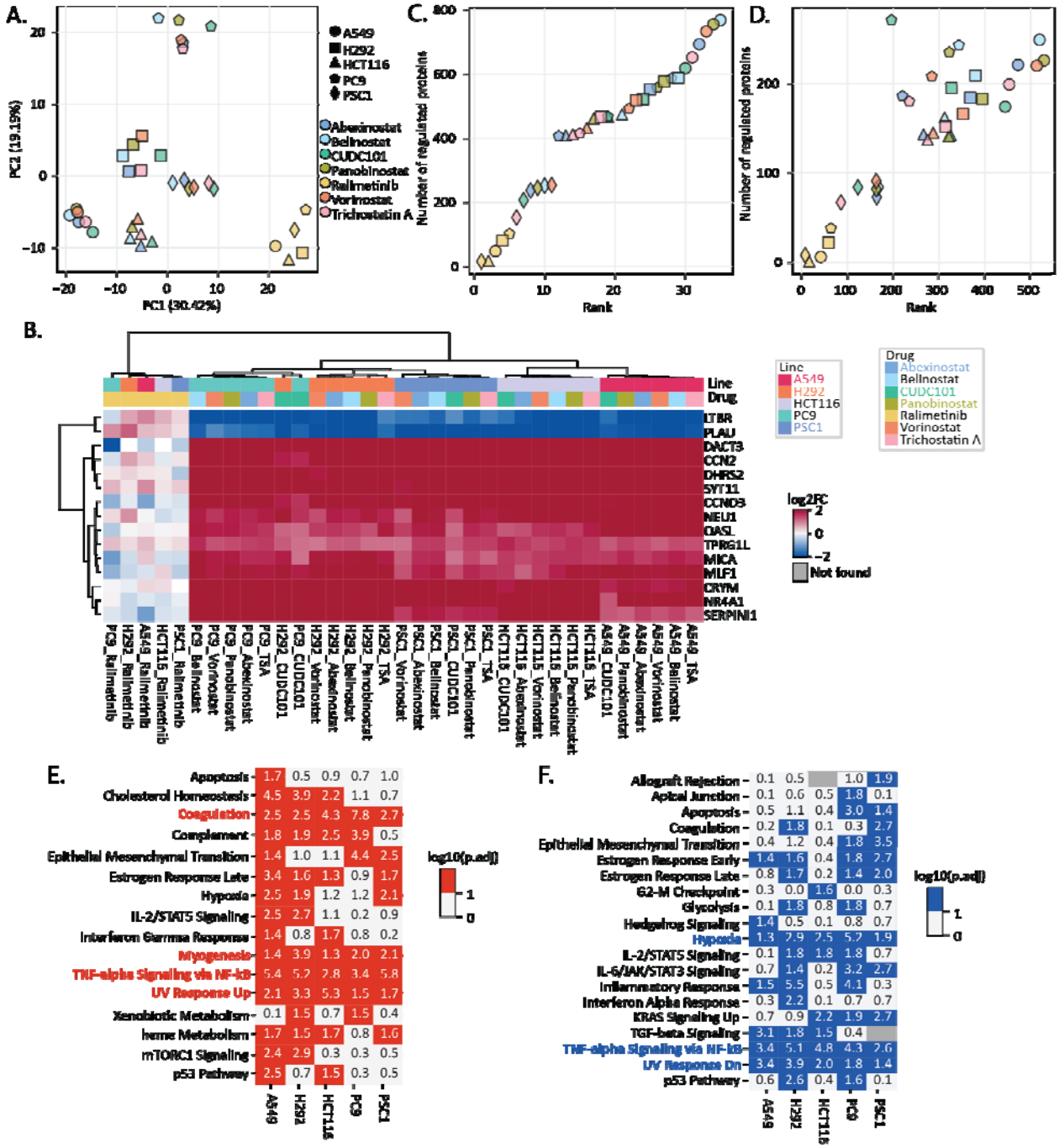

Figure 2 Overall differences between cell lines in response to HDACi or MAPKi. A, Principal component analysis (PCA) of 35 cell-line-by-drug groups. HDACi treated groups were clustered based on cell lines. All ralimetinib treated groups were clustered together (bottom right). Different shapes represent different cell lines. Different colors represent different drug treatments. **B,** Heatmap of log2FC of proteins having abundance changes in all 5 cell lines with all 6 HDACi treatments. The log2FC is the protein abundance change compared with DMSO treatment. **C,** Waterfall plot highlighting the number of

regulated proteins for each cell-line-by-drug group. Figure legend is the same as (**A**). **D,** Activity of each cell-line-by-drug group measured by the number of proteins down-regulated (x axis) and up-regulated (y axis) after 24 h treatment. Regulated proteins are proteins with absolute log2FC > 1. The log2FC is the protein abundance change compared with DMSO. Figure legend is the same as (**A**). **E, F,** Comparison of Hallmark enrichment analysis of regulated proteins from cell lines with HDACi treatment. Left with red color (**E**) is comparison of up-regulated proteins; right with blue color (**F**) is comparison of down-regulated proteins. Regulated proteins are proteins with absolute log2FC > 1. The log2FC is the protein abundance change compared with DMSO. The p-value is calculated by comparing the observed frequency of an annotation term with the frequency that would be expected by chance. The p-value is adjusted by the false discovery rate (FDR). Terms that have an adjusted p-value (p.adj) < 0.05 or log10(p.adj) > 1.3 are considered enriched. Both color scale and numbers represent log10(p.adj).

HDAC-class-specific protein abundance changes in response to HDACi treatment

We next sought to determine what effect HDACi perturbations had on HDAC protein abundance across cell-line-by-drug groups. Based on our quantification of 10 of the 11 human HDAC proteins (Figure 3A), we observed changes in both individual HDAC abundances and more generally in the responses of classes of HDACs. Class I HDACs include HDAC1, 2, 3 and 8, and these are generally found in the nucleus (Y. Li & Seto, 2016). Class II HDACs include HDAC4, 5, 6, 7, 9 and 10, which shuttle between the nucleus and cytoplasm (Y. Li & Seto, 2016). In our analyses, the abundance of Class I HDACs generally did not change after HDACi treatment; conversely, we observed differential abundance for three out of six Class II HDACs (HDAC5/7/9, Figure 3A). This was striking, but also consistent with previous small-scale analyses that found that HDAC7 (Class II), but not HDAC1 (Class I), protein abundance decreased with HDACi treatment (Caslini et al., 2019; Ma & D'Mello, 2011). In general, we found that, when they were altered, HDAC5, HDAC7, and HDAC9 protein abundances decreased upon HDACi treatment. HDAC9 protein abundance went down with HDACi treatment PC9 and PSC1 cells, but had no change in the other three cell lines. Interestingly, the PC9 and PSC1 cells were the most sensitive (PC9) and resistant (PSC1) cells in our viability assay after HDACi treatment (Figure 1C).

Based on these HDAC-class-specific changes, we sought to determine how HDACi treatment remodeled the canonical HDAC regulatory pathway components assembled from literature sources (Shakespear et al., 2011; Suliman et al., 2012). We measured significant abundance changes for 16 proteins from the canonical HDAC pathway (21%; 16/75 proteins, Figure 3B). Among them, the c-Jun transcription factor (JUN) had a significant increase in protein abundance in A549, H292, and HCT116 cells (log_2FC_{A549} = 1.49; log_2FC_{H292} = 1.43; log_2FC_{HCT116} = 1.20), but not PC9 and PSC1 cells (log_2FC_{PC9} = -0.09; log_2FC_{PSC1} = -0.37; Figure 3B, C). By comparison, in our perturbation-based study we observed an anticorrelated relationship between JUN protein abundance and HDAC7 protein abundance (Figure 3D). These data were consistent with previous work demonstrating that HDAC7 inhibits JUN expression and protects neurons from apoptosis (Ma & D'Mello, 2011). Notably, this effect was specific to the analysis of HDACi-perturbed cells there was no significant relationship between JUN and HDAC7 protein abundance in the large-scale CCLE proteomics screen across hundreds of unperturbed cancer cell lines (Nusinow et al., 2020), (Supplementary Figure 3B).

To further explore the proteomic relationships surrounding JUN and HDACi treatments, we expanded the analysis of the HDAC pathway members to also include direct interacting proteins of JUN based on the BioPlex interaction network (Schweppe et al., 2018) (Figure 3C). Within the JUN interaction network, we observed distinct differences in the abundance of the transcription factor JunB which decreased in H292 and PC9 cells (log_2FC_{H292} = -0.84; log_2FC_{PC9} = -1.1), but not in A549, HCT116 and PSC1 cells (log_2FC_{A549} = 0.62; log_2FC_{HCT116} = 0.30; log_2FC_{PSC1} = 0.40). We observed the same trend for c-FOS which forms a heterodimer with JUN and JunB, as c-FOS protein abundance significantly increased in A549,

HCT116 and PSC1 cells (log_2FC_{A549} = 1.82; log_2FC_{HCT116} = 2.5; log_2FC_{PSC1} = 3.62). Interestingly, FOS protein abundance was signficantly anticorrelated with HDAC7 abundance across unperturbed CCLE cell lines (Nusinow et al., 2020). Combination therapies of FOS and HDAC inhibitors have been suggested as a route to enhance the antiproliferative effects of HDAC inhibitors (L. Wang et al., 2022). Yet, our data demonstrate that, owing to cell-type-specific responses, incorporating multiple representative perturbation datasets is necessary to discern the potential responses that may be observed in preclinical studies.

HDAC-proteome co-regulation in response to HDACi treatment

Owing to the large-scale remodeling of the proteome in response to HDACi treatments, we next set out to determine if specific cohorts of proteins or protein complexes demonstrated protein abundance responses that were co-regulated with HDAC protein responses across cell lines. To do this, we calculated the correlation between the 10 HDACs we quantified and the other 5,491 proteins that were quantified in all cell line-by-drug samples (Supplementary table 3). For example, HDAC1 and HDAC2 are known to exhibit partially redundant effects in cells (Y. Zhang et al., 2023), and we observed that HDAC1 and HDAC2 protein abundances were well correlated across datasets ($r_{Pearson}$ = 0.92). From our HDAC co-regulation analysis, we observed 81 proteins with correlated abundances with at least one HDAC protein ($r_{Pearson}$ > 0.9, Supplementary Figure 3A). In keeping with the cell line specific response of HDAC7 to HDACi treatment, we observed 83.9% of these proteins (68 of 81) were correlated with HDAC7 abundance (Supplementary Figure 3A).

Of these proteins, the most highly correlated proteins ($r_{Pearson}$ > 0.95) were SRC, MICALL1 and FUCA1 (Figure 3E, F, G). Again this was striking because comparison of steady state levels of HDAC7 and SRC, MICALL1 and FUCA1 across CCLE cancer cells resulted in a weak anticorrelation of the abundances of these proteins (Supplementary Figure 3C, D, E). The tyrosine kinase SRC is active in non-small cell lung cancers and involved in cellular transformation and metastasis (J. Zhang et al., 2007). Yet, consistent with our proteomics analysis, HDACi treatment can reduce SRC expression in cancer cells (Hirsch et al., 2006). While there was limited functional information about the role of MICALL1 (Molecule Interacting with CasL-like 1) in cancer, MICALL1 protein abundance in response to HDACi treatment was highly correlated with both HDAC7 ($r_{Pearson}$ = 0.96) and SRC ($r_{Pearson}$ = 0.90) protein abundance. While there was no evidence for the direct interactions between SRC, MICALL1, HDAC7, and HDAC5 in the BioPlex interaction network, we found that all of these proteins directly engage with 14-3-3 adapter proteins (YWHAH, YWHAG, YWHAB, YWHAZ, Figure 3H) (Schweppe et al., 2018; Segal et al., 2023; Shen et al., 2020). 14-3-3 proteins are known to regulate the nuclear import of Class IIa HDACs (HDAC4/5/7/9) and stabilize phosphorylated HDAC7 (X. Li et al., 2004; Nishino et al., 2008). While 14-3-3 protein abundances were not significantly changed with HDACi treatment, our data suggest that the alteration of HDAC-related signaling networks was correlated with proteome remodeling and HDACi-mediated effects.

In addition to SRC, MICALL1, and FUCA1, we observed seven cancer-related proteins (Uhlen et al., 2017) with protein abundances that were correlated with HDAC7 (absolute $r_{Pearson}$ > 0.9). These included ARID1A/ARID1B (Lin et al., 2014), bifunctional purine biosynthesis protein ATIC (Trinei et al., 2000), the receptor tyrosine kinase signaling adapter protein GRB2 (Ding et al., 2019; Lowenstein et al., 1992; Yang et al., 2021), phosphatidylinositol 3,4,5-trisphosphate 5-phosphatase INPPL1 (Y.-L. Zhou et al., 2018), methyl-CpG-binding domain protein MBD1 (Wensheng et al., 2019), and retinoic acid receptor RXRG (Joseph et al., 2019) (Supplementary 3F-L). Additionally, we observed that the transcription factor TRPS1 which was known to act upstream of HDACs had increased abundance upon HDACi treatment only in A549 cells (L. Wu et al., 2014). Notably, this was the same cell line (A549) with the largest decrease in HDAC7 protein abundance (Figure 3A). Though many of the HDACi compounds used in our study primarily target both Class I and II HDACs (Y. Li & Seto, 2016), we found that the Class II HDAC7 exhibited robust, but cell-type specific, responses to HDACi treatment across multiple lung cancer cells lines.

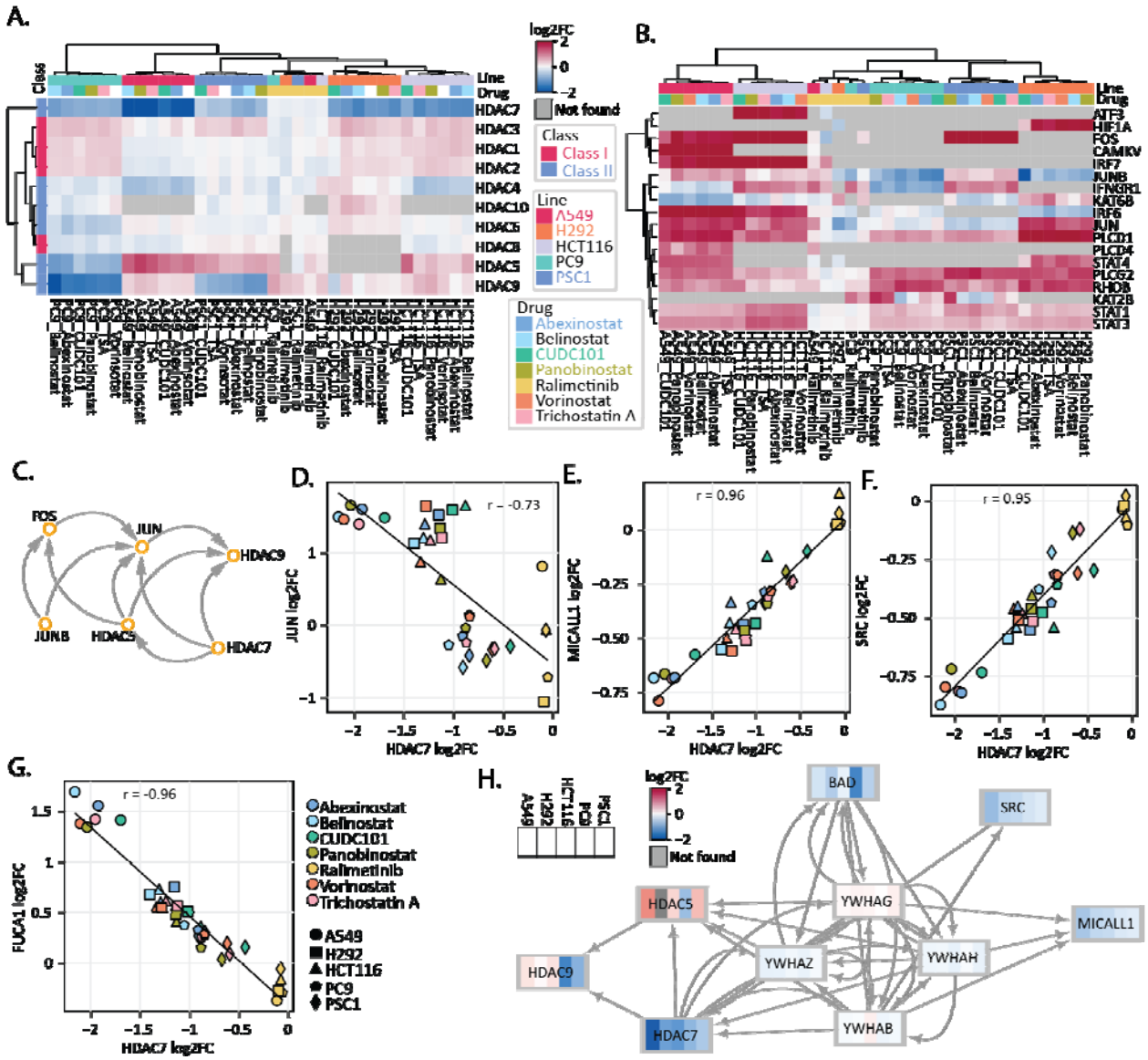

Figure 3 Difference between cell lines of HDACs and proteins from the HDAC pathway. A, Heatmap of log2FC of 10 HDACs found in 35 cell-line-by-drug groups. The log2FC is the protein abundance change compared with DMSO. **B,** Heatmap of log2FC of regulated proteins from a canonical, literature-based HDAC pathway found in 35 cell-line-by-drug groups. Regulated proteins are proteins with absolute log2FC > 1. The log2FC is the protein abundance change compared with DMSO. Heatmap legend is the same as (**A**). **C,** Protein network from Bioplex between HDAC5, 7, 9 and JUN. **D, E, F, G,** Comparison of log2FC of HDAC7 with JUN, MICALL1, SRC or FUCA1. The log2FC is the protein abundance change compared with DMSO. Different shapes represent different cell lines. Different colors represent different drug treatments. Pearson r is labeled on the top of each figure. **H**, Network from Bioplex between 14-3-3 adapter proteins with HDAC5/7/9, MICALL1, SRC and BAD. For each cell line the median log2FC of five HDACi treatments was taken. The log2FC is the protein abundance change compared with DMSO.

Cell signaling response to HDACi treatment positions potential therapeutic interventions

Owing to the widespread remodeling of cell-line-by-drug proteomes and coregulatory protein abundance network surrounding the 14-3-3 phospho-binding proteins, we sought to determine what role cell signaling effectors may be playing a role in cell-line specific responses to HDACi treatment. To this end, we quantified the phosphoproteomes of HDACi treated cells and generated a dataset of a total of 8,787 phosphorylation sites, including 1,363 phosphosites with HDACi-dependent abundance changes (Supplementary data 2). We ranked each cell-line-by-drug group based on the number of regulated phosphosites. PC9 cells treated with HDACi had the largest number of regulated sites, followed by H292, A549, HCT116 and PSC1 cells. This was striking as the PC9 cells were also the most susceptible to HDACi treatments in our cell viability assays (Figure 1C). Interestingly, cell lines treated with ralimetinib had the fewest regulated phosphosites (Figure 4A, Supplementary Figure 4A). Among the 35 cell-line-by-drug groups, 457 phosphosites were only observed to have increased abundance upon HDACi treatment, 526 sites were only observed to have decreased abundance upon treatment, and 190 sites were observed to have both increased and decreased abundance across cell-line-by-drug groups (Figure 4B, 4C). We then explored HDACi regulated events based on phosphosites which were regulated with no corresponding change in protein abundance (phospho-specific regulation). In total, we observed 1,622 phospho-specific effects for 975 proteins (Supplementary Figure 4A). Consistent with the cell-cycle effects of HDAC inhibition, we observed phospho-specific regulation enriched for the G2-M checkpoint and mitotic spindle in all 5 cell lines (Supplementary Figure 4B, C).

As with the co-regulatory analysis of protein abundances, we found that 681 phosphosites quantified in at least 28 cell-line-by-drug groups were correlated with the abundance of just HDAC5, HDAC7, and HDAC9 (Figure 4D). Of these, we observed 12, 11, and 4 phosphosites to be correlated with HDAC5, HDAC7, and HDAC9, respectively protein abundance ($r_{Pearson} > 0.8$; Figure 4E, Supplementary Figure 4D, 4E). Among them, phosphorylation of BAD Ser118 was significantly negatively correlated with HDAC7 ($r_{Pearson} = -0.86$, Figure 4F), while BAD protein abundance was not ($r_{Pearson} = 0.13$). BAD's pro-apoptotic activity requires heterodimerization to protein binding partners Bcl-2 and Bcl-xL (Gajewski & Thompson, 1996). BAD Ser118 phosphorylation disrupts Bcl-2/Bcl-XL binding, driving engagement of 14-3-3 proteins to enable dispersion of BAD away from mitochondria and increasing cell growth (Datta et al., 2000; Lizcano et al., 2000; J. Mann et al., 2019). Interestingly, the HDACi-dependent increases in Ser118 abundance were observed in all three cell lines with intermediate sensitivity to HDACi (A549, H292, HCT116; Figures 1C, 4G). These data point to a relationship between HDAC activity (and HDACi inhibition), HDAC abundance, and a BAD-dependent mechanism by which specific cell lines attempt to overcome HDACi-mediated cell death.

To investigate this further, we sought to determine which kinases may be responsible for the HDACi-dependent phosphorylation of BAD in our tested cancer cell lines. Previous work demonstrated that Ser118 can be phosphorylated by PKA (Datta et al., 2000), RSK (Tan et al., 2000), and in vitro by AKT1 (Datta et al., 2000). To identify which kinase was likely driving HDACi-mediated phosphorylation of BAD Ser118, we measured the correlation between BAD Ser118 and the 248 protein kinases that were quantified in at least 28 samples in our HDACi-treatment dataset. Seven kinases had abundance profiles that correlated with BAD Ser118 ($r_{Pearson} > 0.8$, Figure 4G). These included MARK4, NRBP2, AKT1, SRPK2, PDK2, RPS6KC1, ADCK5, and MKNK1. Based on the 'RR-x-S' motif surrounding BAD Ser118, KinasePredictor (Poll et al., 2024) suggested that AKT1 ($score_{KinasePredictor}$=1.84), SRPK2 ($score_{KinasePredictor}$=1.59), and MARK4 ($score_{KinasePredictor}$=0.58) were likely candidates for the acting kinase upstream of Ser118 (Poll et al., 2024; Sugiyama et al., 2019). Combined with findings that AKT1 can phosphorylated Bad Ser118 in vitro, these data suggest that combination treatment of lung cancer cells with both an HDACi and an AKT1 inhibitor may be a route to improving responsiveness to HDACi-treatment in lung cancer cells. This would be consistent with the sensitization of lung cancer cells to

HDACi through combination therapies with receptor-tyrosine kinase inhibitors that act upstream of AKT1 (Piao et al., 2016) and vice versa (D. Wu et al., 2021).

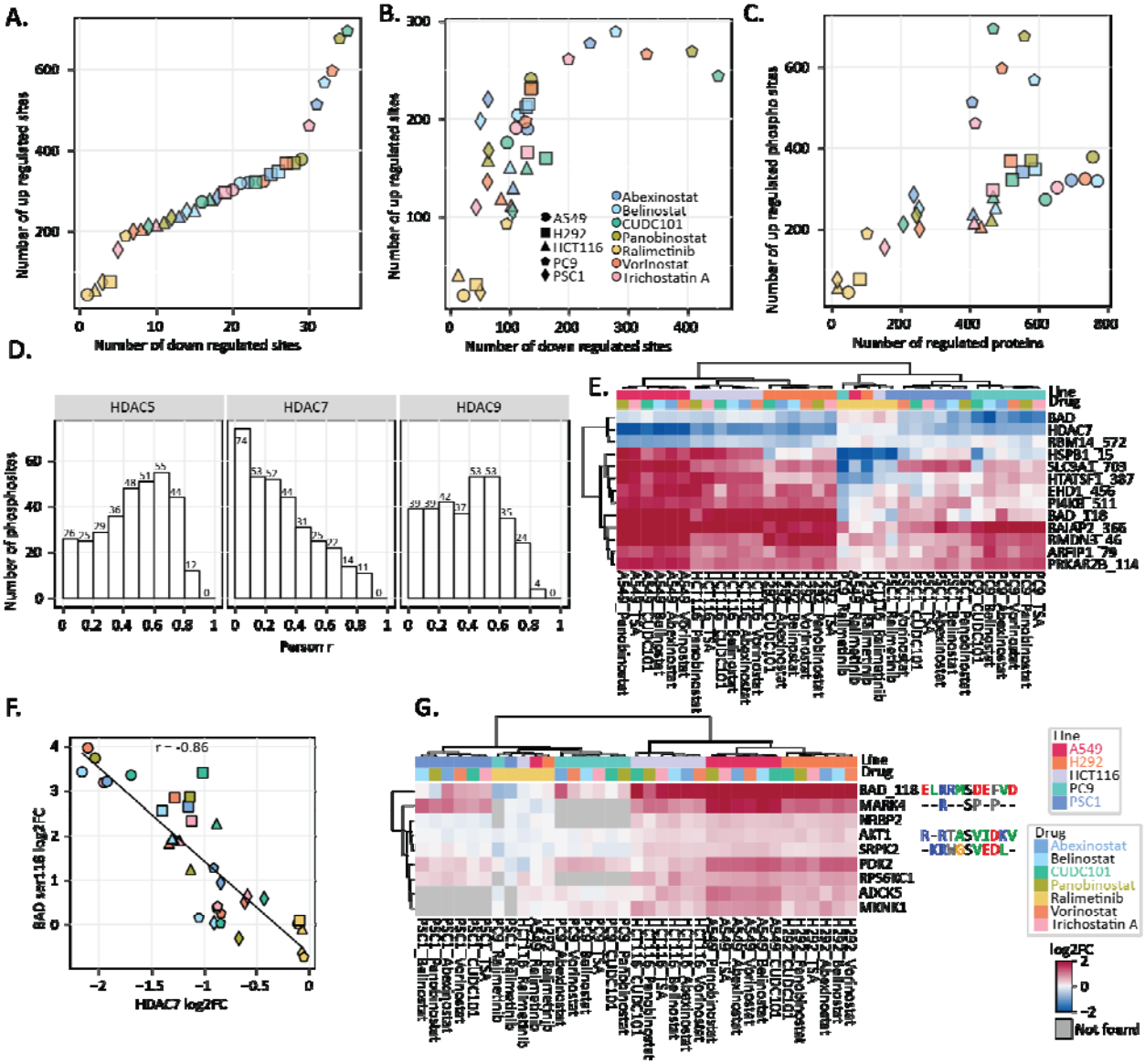

Figure 4 Difference between cell lines of phosphorylation with HDACi treatments. A, Waterfall plot highlighting the number of regulated phosphosites for each cell-line-by-drug group. Legend is the same as (**B**). **B,** Activity of each cell-line-by-drug group measured by the number of phosphosites down-regulated (x axis) and up-regulated (y axis) after 24 h treatment. Regulated phosphosites are phosphosites with absolute log2FC > 1. The log2FC is the phosphorylated peptide abundance change compared with DMSO. Different shapes represent different cell lines. Different colors represent different drug treatments. **C,** Activity of each cell-line-by-drug group measured by the number of regulated proteins (x axis) and regulated phosphosites (y axis) after 24 h treatment. Regulated proteins or phosphosites are proteins or phosphorylated peptides with absolute log2FC > 1. The log2FC is the protein abundance or phosphorylated peptide change compared with DMSO. Phosphorylated peptides were matched to proteins. Legend is the same as (**B**). **D,** Number of phosphosites correlated with HDAC5, HDAC7 and HDAC9 protein abundance. **E,** Heatmap of log2FC phosphosites correlated to HDAC7 with absolut pearson r > 0.8. The log2FC is the phosphorylated peptide abundance change compared with DMSO.

Heatmap legend is the same as (**G**). **F,** Comparison of HDAC7 protein abundance log2FC compared with DMSO treatment and BAD ser118 peptide abundance log2FC compared with DMSO treatment. Pearson r is labeled on the top of the figure. Legend is the same as (**B**). **G,** Heatmap of log2FC of kinases correlated to BAD Ser118 with absolute pearson r > 0.8. The log2FC is the protein or phosphorylated peptide abundance change compared with DMSO. BAD amino acids 113 to 123 were shown with ser118 in the middle. Three kinases, MARK4, AKT1, and SRPK2, have information about substrate motifs. Serine is aligned.

Coordinated remodeling of the transcriptomes and proteomes of HDACi perturbed cells

Owing to the fact that HDAC perturbation directly affects cellular transcription, we next sought to understand the level of concordance between the transcriptome and proteome effects downstream of epigenetic perturbation of lung cancer cells. We compared our A549 perturbed proteomics data of established A549 transcriptome data for matched cell and treatment conditions (Srivatsan et al., 2020). Cell responses generated distinct clusters based on treatments on both single-cell level and bulk level (Figure 5A, Supplementary Figure 5A). We pseudo-bulked these single-cell data for comparison to our bulk proteomics analyses (Figure 5B, Supplementary Figure 5B). In response to HDACi treatments, A549 cellular proteomes and transcriptomes were correlated ($r_{Pearson}$ = 0.48-0.64) (Figure 5B), consistent with previous proteomics and transcriptomics comparisons ($r_{Pearson}$ = 0.42-0.57) (D. Wang et al., 2019). For example, panobinostat treatment resulted in consistent molecular responses for both the proteome and the transcriptome in A549 cells ($r_{Pearson}$ = 0.64). We then grouped protein and transcript responses to HDACi treatment into nine groups based on significant changes in proteomic and transcriptomic responses—e.g., Group 1 had increased transcript expression decreased protein abundance with HDACi treatment while Group 3 had concordant increased transcript expression and increased protein abundance with HDACi treatment (Supplementary Figure 5B).

Concordant transcript and protein responses to HDACi treatment in Groups 3 and 7 were observed for 505 protein/transcript pairs. As expected, the proteins in these groups were enriched for oncogenes and tumor suppressors, with notable effects of increased abundance of JUN, FOS and CDKN1A, and reduced abundance of HDAC7 and CCNA2 (Figure 5B). We then defined discordant protein/transcript pairs in Groups 1, 4, 6, and 9—i.e., those with differential abundance of proteins with HDACi treatment, and no effect on the transcripts, or vice versa (Figure 5B). As such, we found that Cyclin D3 (CCND3) was discordantly regulated at the protein and transcript level in response to HDACi treatment with increased protein abundance after HDACi treatment (Figure 5C), but decreased transcript expression (Figure 5B). The increased relative abundance of CCND3 protein but not transcripts suggests HDACi-mediated post-translational control of CCND3. Since CCND3 coordinates cell cycle progression through binding and activation of CDK4/6 kinase, one route for post-translational control of CCND3 could be through stabilization of the CDK4/6-CCND3 protein complex (LaBaer et al., 1997; Bockstaele et al., 2006; Sawai et al., 2012). We also found that CDK6, but not CDK4, protein abundance decreased in A549 cells with HDACi treatment (Figure 5C). Thus, in response to HDACi-mediated CDK4/6 inhibition through increased expression and abundance of CDKN1A, this suggests that lung cancer cells may stabilize the CDK4-CCND3 complex interaction to maintain cell viability and overcome HDACi-mediated reduction in CCND3 transcript production (J. Hu & Colburn, 2005).

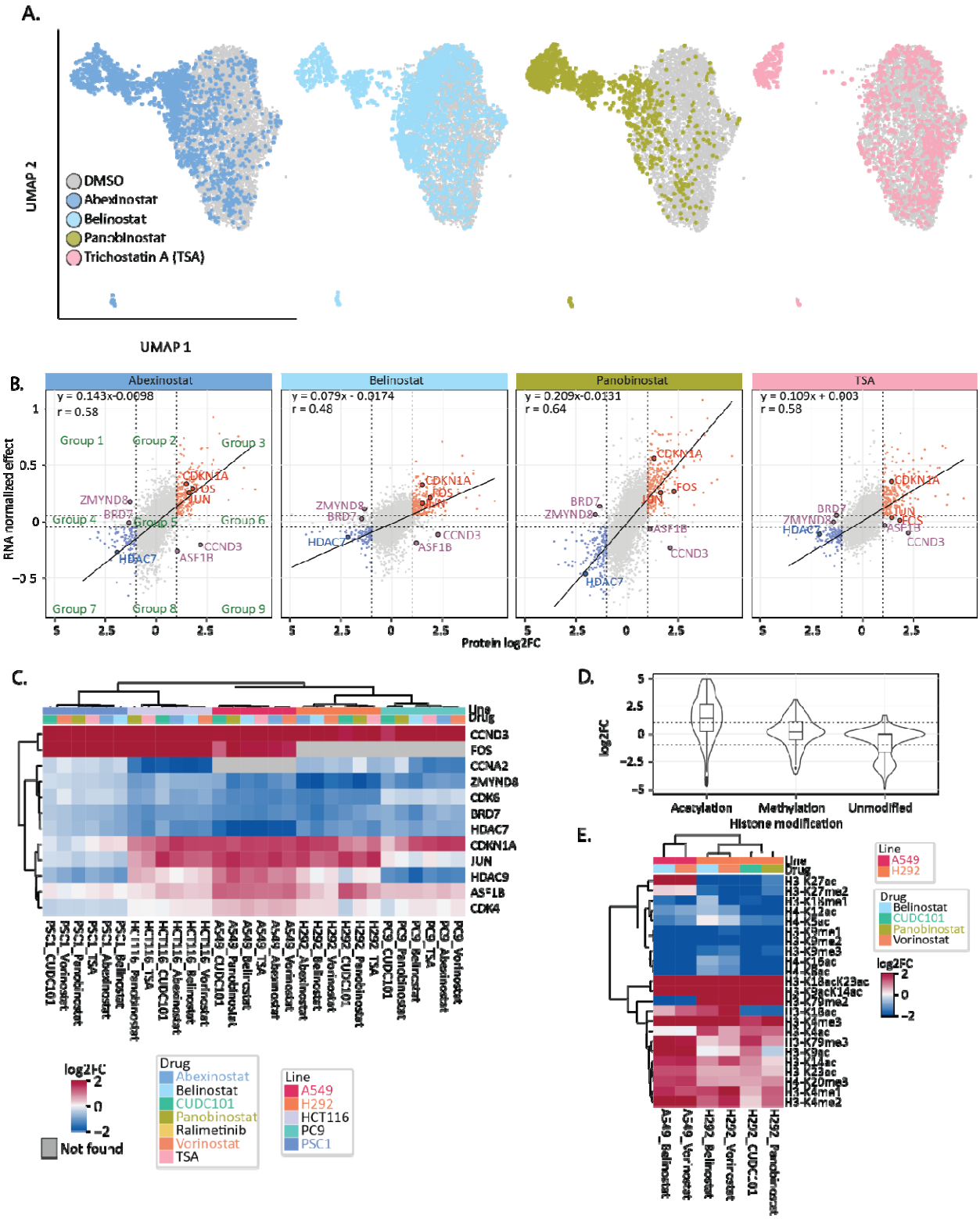

Figure 5 Coordination between transcriptomes, proteomics and histone modification in A549 with HDACi treatments. A, UMAP analysis of single-cell transcriptomics in A549 with 4 HDACi, abexinostat, belinostat, panobinostat and TSA. **B,** Activity of A549 treated with 4 HDACi by the protein abundance log2FC (x-axis) compared with DMSO and RNA normalized effect (y-axis). The regulated proteins were defined as absolute log2FC > 1 in the proteomics dataset and absolute normalized effect >

0.05 in transcriptome dataset. Based on the four thresholds, proteins were grouped into 9 clusters. **C,** Heatmap of protein abundance log2FC of discordant proteins. Discordant proteins were proteins found in cluster 1,4,6 and 9, that contain proteins with log2FC > 1, but RNA normalized effect < 0.05, or proteins with log2FC < -1, but RNA normalized effect > -0.05. **D,** violin plot of log2FC of histone modifications. The log2FC is the abundance change of histone peptide with modifications compared with DMSO (center line: median; upper box limit: third quartile; lower box limit: first quartile; whiskers: 1.5x interquartile range; points: outliers). **E,** Heatmap of log2FC regulated histone modification in A549 and H292 with HDACi treatments. The log2FC is defined in (**D**).

Coordinated remodeling of histone modification and proteomes of chemically perturbed cells

Based on the pleiotropic effects we observed at the proteomic and transcriptomic levels and owing to the relationship between HDACi and histone modification status, we sought to determine the relationship between specific histone modifications in response to HDACi and the protein phenotypes we observed. To measure the extent of histone modification state changes we quantified specific histone marks and unmodified peptides after histone extraction in both H292 and A549 cells (Z.-F. Yuan et al., 2015). As expected after HDACi treatment, histone acetylation generally increased, while the relative abundance of histone methylation events decreased (Figure 5D). For example, the abundance of both singly-modified H3K18ac and doubly-modified H3K18ac-H3K23ac increased with HDACi treatment. Indeed, the majority of histone modifications, e.g., H3K4me1 and H3K14ac, were consistent in both A549 and H292 cells (Figure 5E). Strikingly, we also observed cell line-specific HDACi-mediated effects on histone modifications. Specifically, while we found that H3K27ac abundance increased as expected in A549 cells treated with HDACi, H3K27ac abundance decreased in H292 cells treated with HDACi. Similarly, H3K79me2 had increased abundance in H292 cells upon HDACi treatment, yet HDACi treatment reduced H3K79me2 abundance in A549 cells (Figure 5E). As H3K79 methylation has been demonstrated to antagonize modification of H3K27 (S. Chen et al., 2015), these data were consistent with cell lineage-specific antagonism between H3 modifications. We note that the protein abundances of known histone methyltransferases did not change in either cell line—e.g., SETD2 which is associated with H3K36 methylation (Xie et al., 2022), or EZH1 and EZH2 which are associated with H3K27 methylation (Nichol et al., 2016). Thus, antagonism of histone methylation status would likely not have been due to a shift in protein abundance upon HDACi treatment, but, more likely, an alteration of methylation/acetylation activity (W. Yuan et al., 2011).

Dissecting discordant proteome and transcriptome responses for histone binding proteins

In addition to CCND3 mentioned above, we observed discordant transcript/protein relationships for chromatin binding factors ASF1B, ZMYND8, and BRD7 (Figure 5B). These findings were especially interesting since transcript abundance for ASF1B were found to have prognostic value for cancer outcomes (Corpet et al., 2011). Notably, each of these proteins has been shown to directly interact with specific histones and histone modifications (Adhikary et al., 2016; Alvarez et al., 2011; Cong et al., 2006; N. Li et al., 2016; Mukherjee et al., 2020). Thus, we compared the HDACi-mediated responses for ASF1B ZMYND3, and BRD7 with histone modification states driven by differential histone modification states in matched cells.

Quantitation of histone state allowed us to compare histone modifications known to be bound by ASF1B, ZMYND8, and BRD7. The histone chaperone ASF1B recognizes H3K9me1 and imports H3 into the nucleus, where ASF1B can form a complex with H3K14K18ac (Alvarez et al., 2011). We found that H3K9me1 decreased in A549 cells treated with belinostat or vorinostat treatment, while H3K14ac and H3K18ac increased (Figure 5E). We then compared HDACi-mediated effects on histone modifications state across both H292 and A549 cells to determine if cell line-specific differences in histone modification status might be related to the discordant transcriptional and post-translational measurements for ASF1B. Since previous work demonstrated that ASF1B complexes can interact with H3K27ac and

H3K79me2 (Jasencakova et al., 2010), it was striking to find that HDACi treatment resulted in increased H3K27ac in A549 cells, but decreased H3K27ac in H292 cells (Figure 5E). Although the transcript abundance of ASF1B did not change significantly, we speculate that ASF1B may be sequestered in the nucleus owing to hyperacetylation of H3K18 and thus be protected from degradation. ASF1B overexpression is known to promote proliferation of cancer cells in a CDK9-dependent manner (X. Liu et al., 2020). Yet, from our data, we observed no significant change in CDK9 protein abundances (log2FC between -0.4 and 0.1, Supplementary Data 1) corresponding with the ASF1B protein abundance shifts. These data hint at a CDK9-independent route by which ASF1B stabilization in cancer cells may play a role in bypassing the effects of HDAC inhibition—in addition to BAD Ser118 phosphorylation noted above.

Like ASF1B, ZMYND8 recognizes multiple histone marks, including H3K4me1/H3K14ac or H3K36me2/H4K16ac and has been associated with suppression of tumor-related genes (Adhikary et al., 2016; N. Li et al., 2016; Mukherjee et al., 2020). BRD7 can bind to H3K14ac (Cong et al., 2006) and predominantly localizes to the nucleus where it has been shown to suppress tumor proliferation (M. Zhou et al., 2006). However, we noted that the protein abundance for both ZMYND3 and BRD7 decreased with HDACi treatment, which was inverted from the phenotype we observed for ASF1B (Figure 5C). Since all of these proteins can recognize H3K14ac, our data may suggest that the increased abundance and thereby the potential to occupy H3K14ac sites could exclude ZMYND3 and BRD7 inhibiting their ability to suppress tumor proliferation genes (K. Hu et al., 2019).

Protein-drug engagement indicates potential mechanistic routes for divergent cellular responses

Having leveraged to dissect the differential effects for key histone modifications in response to HDACi perturbation across cell lines, we next aimed to determine which proteins directly engaging with HDAC inhibitors to drive molecular remodeling of cancer cell lines. To do this we performed thermal stability analyses of HDACi treated A549 cells (Gaetani et al., 2019; Van Vranken et al., 2024) (Figure 6A). Owing to the potential importance of protein, cellular, and chromatin context in affecting HDACi engagement, we performed these assays in both cells and lysates to confirm protein-engagement data and determine likely direct versus indirect HDACi relationships (Van Vranken et al., 2024). We then compared our HDACi proteomics and thermal stability analyses to integrate understanding of HDACi engagement versus cellular remodeling (Figure 6B, C, Supplementary Figure A, B, C).

Thermal stability analysis revealed clear engagement of belinostat and vorinostat with HDAC1, HDAC2, and HDAC6 (Figure 6B). Thus, coupled with our quantification of increased H3K27ac, and purely from unbiased proteomics analyses, we could recapitulate the canonical HDACi mechanism of action (Figure 5B). In keeping with our speculation that HDACi-protein engagement may drive cell line-specific responses, we also observed off-target protein engagement of HDACi compounds. These included HDACi engagement with cancer-related proteins such as defender against cell death 1 (DAD1) and the cell cycle kinase AURKB (Figure 6B). DAD1, a putative cancer prognostic marker (Uhlen et al., 2017), was significantly stabilized by belinostat in both cell- and lysate-based thermal stability assays (Figure 6B). DAD1 is an anti-apoptotic protein (Sugimoto et al., 1995) and a component of the oligosaccharyltransferase complex (Roboti & High, 2012). In addition to DAD1, the cell cycle kinase AURKB was significantly destabilized with HDACi treatment in both cell- and lysate-based thermal stability analyses (Figure 6B). Based on molecular docking, belinostat can bind the AURKB active site in a similar pose to the binding of the AURKB inhibitor VX-680 (Figure 6D)[REF]. From our viability assay, A549 cells were more sensitive to belinostat than any other HDACi and this compound-specific sensitivity was not seen for the other KRas mutant cell line (HCT116) or the other moderately sensitive cell line (H292, Figure 1C). Our belinostat-engagement data suggest that the differences in viability may be related to differences in AURKB steady-state total protein abundances. Between A549 and H292 cells, AURKB protein abundance was 5.7-fold lower in A549 cells [REF - Nusinow CCLE], potentially making A549 cells especially sensitive to off-target inhibition of AURKB. Together, the integration of HDACi

engagement data enabled dissection of potential non-canonical mechanisms of lineage specific effects in response to HDACi.

Finally, measurement of HDACi engagement did not correspond with changes in the total protein abundance of the same protein in response to HDACi treatment (Figure 6C). Based on differences between protein and stability and our previous work demonstrating that thermal stability analyses could recover 'secondary' protein interacting partners (Van Vranken et al., 2024), we set out to identify HDACi-mediated protein complex alteration. From our thermal stability analyses, belinostat engaged HDAC1 and HDAC2, but had no effect on the total protein abundance for either protein (Figure 6D). At the complex level, we observed HDACi-mediated destabilization of variant polycomb repressive complex components MGA and EHMT1/2 (Figure 6D, 6E) and HDAC1/2 are components of the same variant of the polycomb repressive complex PRC1 (PCGF6) (Blackledge & Klose, 2021). These data suggest that while HDACi treatment does not affect the total abundance of either polycomb component (Figure 6D), that the assembled PCGF6 variant complex is disrupted with HDACi treatment. Similarly, thermal stability analysis revealed secondary effectors of HDACi treatment with ZMYM3. The zinc finger protein ZMYM3 was destabilized and the protein abundance decreased in cells after belinostat treatment (Figure 6D). ZMYM3 is a component of another HDAC complex, the BHC histone deacetylase complex that includes HDAC1/2 (Hakimi et al., 2003; Leung et al., 2017). Thus, HDACi-mediated changes in thermal stability enabled detection of complex-specific secondary effectors of HDACi treatment that were directly related to the canonical mechanism of action.

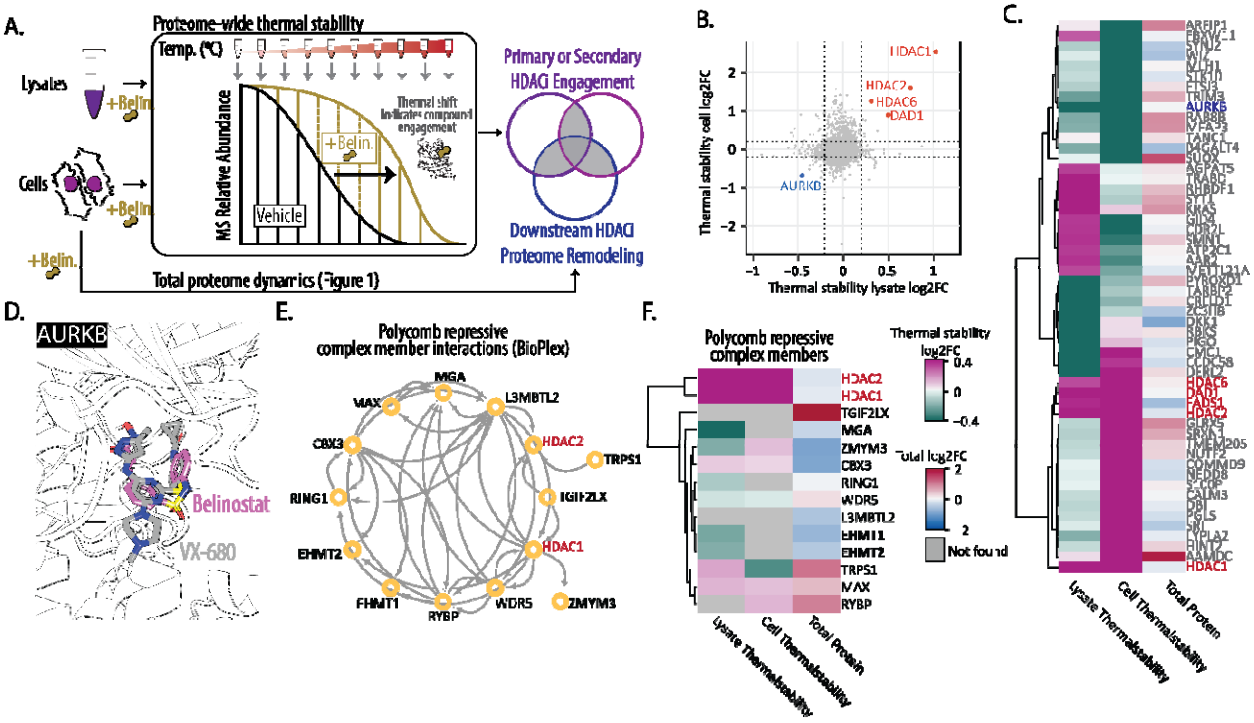

Figure 6 Analysis for protein-drug engagement for divergent cellular responses. A, Diagram shows cell and lysate thermal stability analyses and total proteome were performed using A549 cells or lysates treated with 10μM belinostat. **B,** Comparison between two thermal stability of A549 with belinostat treatment. The log2FC is the protein abundance compared with DMSO. **C,** Heatmap of log2FC of proteins that were significantly stabilized or destabilized in cell-based and lysate-based thermal stability assays, but not significant based on the protein abundance changes in total proteomics. Stabilization and destabilization were defined as protein abundance log2FC compared with DMSO in thermal stability assay larger than 0.2 (stabilized)/smaller than -0.2 (destabilized). The significant protein abundance changes are defined as absolute log2FC > 1 in total proteomics. **D,** Molecular docking of belinostat (pink)

and AURKB (white ribbon, PDB: 4AF3). Positioning of belinostat in the ATP-competitive binding pocket of AURKB was consistent with binding of the AURKB-targeted inhibitor VX-680 (Elkins et al., 2012). **E,** BioPlex protein interaction network for components of the polycomb repressive complex (PRC1). **F,** Heatmap of log2FC thermal stability and proteome responses for members of PRC1.

Discussion

Disparate cell states within cancer cells, driven by differential genetics, signaling axis activation, and protein interactions lie at the heart of inconsistent outcomes for therapeutic treatments. We investigated this phenomena in the context of pleiotropic epigenetic (HDAC) inhibition as a model. HDAC inhibitors are actively used clinically for hematological malignancies and also promising preclinical activities for solid tumors, but with disputed efficacy based on cancer type and known adverse effects (Mamdani & Jalal, 2020). Our multi-omic study demonstrates that it is essential to comprehensively characterize the molecular outcomes of therapeutic intervention that represent the diversity of molecular starting points (e.g., genetic backgrounds). In the context of lung cancer cell models, the majority of available lung cancer cell lines commonly used for lung cancer studies and pre-clinical drug testing have a remarkable imbalance of race and gender, which call for action to establish omics resources to characterize these heterogeneous responses to drugs (Leon et al., 2023). Ignorance of the heterogeneity of lung cancers in drug therapy may lead to inconsistent clinical trial results, although the preclinical results may look promising (Mamdani & Jalal, 2020).

At the outset of this work, several large databases already existed for the characterization of diverse in human cancer cell lines, such as recent chemical genomic screens (Srivatsan et al., 2020) and the proteogenomic characterization of cell lines from the Cancer Cell Line Encyclopedia (CCLE) (Ghandi et al., 2019; Nusinow et al., 2020). Here, we sought to extend these valuable resources which focused on steady-state proteomes by tracking how proteome remodeling after exposure to drug perturbation. We compared our lung cancer specific proteomics data with recent databases describing mechanistic annotation of drugs by profiling proteomics data, such as DeepCoverMOA (Mitchell et al., 2023), and the decrypt datasets (Eckert et al., 2024; Zecha et al., 2023). In shared cell-by-drug sample sets with these datasets, we observed consistent HDACi perturbation effects on the abundance of CDKN1A and CCND3 (Richon et al., 2000; Siavoshian et al., 2000); increased abundance of JUN protein and decreased abundance of HDAC7 (Ma & D'Mello, 2011); and reduced abundance of CCNA2 (Majumdar et al., 2012). As expected, proteins with reduced abundance were largely associated with the regulation of transcription. For example, the increased abundance of JUN in A549, H292 and HCT116 cells, but not regulated in PC9 cells, correlated with PC9 cells' poor viability with HDACi treatment. Upregulation of JUN is associated with cell proliferation and differentiation (Papavassiliou & Musti, 2020), which could explain PC9 is more sensitive to HDACi. Second, owing to the use of a single cancer cell line in many of these studies (Eckert et al., 2024; Mitchell et al., 2023), our data added a new level of understanding for how non-isogenic cell lines respond to chemical perturbation. Building on this work, the data presented here provides a molecular landscape for how cancer cell lines behave when they are treated with epigenetic inhibitors, and how this information can be leveraged to understanding the molecular remodeling of cancer cells in response to therapeutic treatments. As such, these data serve as a rich resource for hypothesis generation to determine the consequences of diverse cellular responses to small-molecule therapies.

To demonstrate the utility of these data as a resource, we explored the non-negligible differences in drug responses across various lung cancer cell lines through proteome profiling of five distinct lines by integrating proteomics, phosphoproteomics, and histone modification data. By combining proteomics with thermal stability data and transcript profiles, we were able to identify specific protein and protein complex effectors of HDACi treatment in lung cancer cells (e.g., polycomb variant PCGF6). HDACi

engagement data also revealed potential mechanisms of HDACi, such as through the engagement of DAD1 and AURKB. Similarly, profiling histone modifications empowered hypothesis generation concerning a potential interaction model between ASF1B and histone modification. Discordant changes of transcript and protein abundance provided revealed multiple routes by which cells can compensate for HDACi initiated cell death. We extended this work to show that abundance changes for specific histone modifications correlated with protein and/or transcript abundance for cell cycle and chromatin regulators CCND3, ZMYND8, ASF1B, and BRD7. For the zinc finger ZMYND8 we note that only through the comparative transcriptomic and proteomic analysis did this protein become a strong candidate for future work owing to the moderate decrease in protein abundance but a discordant increased transcript abundance. These findings together deepen our understanding of HDACi and influence their application in clinical practice.

Multi-cell line proteomics responses to HDACi can uncover relationships between cancer driver genes and drug responses. EGFR is the most common oncogene for NSCLC (LoPiccolo et al., 2024; F. Zhou & Zhou, 2018). PC9 cells have an EGFR gain of function mutant (Nagai et al., 2005), and it was thus consistent that PC9 cells had low cell viability with CUDC-101 treatment. Yet, PC9 cells were also generally the most sensitive to HDACi treatment. The HDACi-responsive phosphoproteome of PC9 cells had distinct differences with other cell lines: it had more down-regulated proteins than up-regulated proteins, and more regulated phosphosites with HDACi treatments. PC9 cells had the greatest number of unique regulated proteins, yet, these effects in PC9 cells do not concentrate in specific pathways. Conversely, HDACi treated A549 cells had fewer unique regulated proteins than PC9, but the A549 response proteins were largely clustered in nine pathways. Thus, although this dataset focuses on HDAC inhibition, extension of our multiomics approach to include additional epigenetic drugs, larger cohorts of diverse cell lines, and improved methods to enhance throughput would empower our understanding of key effectors of heterogeneous molecular responses in cell models.

Method

Cell culture conditions

A549 (CVCL_0023), H292 (CVCL_0455), HCT116 (CVCL_0291), PC9 (CVCL_B260), and PSC1 (CVCL_5622) cells were dispensed into tissue culture treated 96 well plates at a density of 37,500 cells per well in a volume of 200 μl. After 24 h, cells growing at less than 80% confluence were then treated with 10 μM of each drugs, including abexinostat, belinostat, CUDC-101, trichostatin A (TSA), panobinostat, vorinostat (SAHA), and ralimetinib, or 0.1% DMSO. All treatments were performed in 6 replicates: 2 replicates for proteome analysis, 2 replicates for viability analysis and 2 replicates for BCA assay. after treatment, cells were incubated for 24 h at 37 °C before washing with 200 μl PBS per well. After all PBS was aspirated, clear cell culture plates were immediately used for sample preparation for proteomics analysis or viability assay. Viability assay was performed with CellTiter-Glo® Luminescent Cell Viability Assay (Promega).

Sample preparation for proteomics analysis

Sample lysis, reduction, alkylation, SP3 and digestion were processed with liquid handler OT2. Lysis buffer for BCA assay contains 8 M urea, 50 mM NaCl, 200 mM EPPS pH 8.5, Roche protease inhibitor tablets. Lysis buffer for proteomics analysis contains 5 mM TCEP in addition for protein reduction. Lysis buffer 30 μl was added into each well, followed by shaking at 500 rpm for 30 min. Protein concentrations were measured using Pierce BCA assay kits. Proteins for proteomics analysis were then alkylated with 30 μl 10 mM iodoacetamide for 30 min in the dark. The alkylation reaction was quenched by adding an additional aliquot of DTT. Proteins were then transferred to a 96-well PCR plate before being isolated using SP3. In brief, 2 μl of each bead type was added to each well before adding 65 μl neat ethanol and shaking for 30 min at 1000 rpm. Samples were placed on a magnet rack and supernatant was aspirated.

Beads were washed with 125 µl 80% ethanol three times by resuspending. Beads were resuspended in 40 µl digest buffer (200 mM EPPS pH 8.5, 20 ng µl-1 LysC), then incubated overnight at 37 °C with constant agitation, before adding trypsin (400 ng) for an additional 6 hr at 37 °C. The final concentration of peptide was about 1 µg/µl. Two replicates of each cell line were manually labeled with a set of TMTpro 16-plex reagents, and the mixture was incubated at room temperature for 1 h. The reaction was quenched with 0.5% hydroxylamine, before pooling beads and eluates into a single 2 ml tube and placing it on a magnetic rack. Supernatant was collected. After labeling and mixing, peptide mixtures were desalted using C18 sep-pak cartridges (50 mg, Waters).

For phosphopeptide enrichment, PureCube magnetic beads were used with modified protocol (Leutert et al., 2019). In brief, peptides were dissolved in 80% ACN, 0.1% TFA and mixed with beads, shaking for 30 min. phosphorylated peptides were eluted with 50% ACN, 2.5% NH4OH and then neutralized with 75% ACN, 10% formic acid. Elutes were desalted via Stage-tips prior to mass spectrometry analysis. Flow-throughs were then fractionated using basic-pH reverse phase chromatography (Navarrete-Perea et al., 2018). Briefly, peptides were resuspended in Buffer A (10mM ammonium bicarbonate, 5% acetonitrile, pH 8) and separated on a linear gradient from 13% to 42% Buffer B (10mM ammonium bicarbonate, 90% acetonitrile, pH 8) over an Agilent 300Extend C18 column using an Agilent 1260 HPLC equipped with wavelength detection at 214 nm and 254 nm). Fractionated peptides were desalted using Stage-tips prior to mass spectrometry analysis.

Sample preparation for protein thermal stability assay

Thermal proteome profiling (TPP) by protein integral solubility assay (PISA) was performed as previously described (Van Vranken et al., 2024). Each PISA experiment was performed in triplicate.

For live-cell PISA treatment, A549 cells were grown to a density of 1 x 10^6 cells/mL, isolated by centrifugation, and resuspended in fresh media to 6 x 10^6 cells/mL. to each well of a 24-well plate was added 500 uL of cell suspension and 1 mL of treatment (or vehicle) in media for a final cell concentration of $2x10^6$ cells/mL and a final treatment concentration of 10 µM. Cells were incubated with treatment for 1 hr at room temperature. 1 mL from each incubated sample ($2x10^6$ cells) was collected, washed once in PBS, and resuspended in PBS containing 10 µM treatment. For each treatment condition, 30 µL of sample was aliquoted into 10 wells of a PCR plate and subjected to a temperature gradient from 48°C to 58°C for 3 minutes, then allowed to cool to room temperature for 5 minutes. 30 µL of ice-cold lysis buffer (200 mM EPPS pH 7.2, 150 mM NaCl, Roche cOmplete protease inhibitor, 0.5% NP-40) was added to each PCR plate well. 50 µL from each temperature point of a single condition was collected and pooled and cells were allowed to lyse at 4°C for 15 minutes. Lysate was spun at maximum speed for 2 hours and the soluble fraction was collected for sample preparation for proteomic analysis.

For lysate PISA treatment, cells were resuspended in the lysis buffer as above and lysed by repeated aspiration through a 21-gauge needle. Lysate was centrifuged at maximum speed for 30 minutes at 4°C. The soluble fraction was separated and lysate protein content was determined by BCA. Lysate and treatment were combined in lysis buffer for a final protein concentration of 1 mg/mL and a treatment concentration of 10 µM and then incubated at room temperature for 15 minutes. For each treatment condition, 30 µL of sample was aliquoted into 10 wells of a PCR plate and subjected to a temperature gradient as above. 25 µL from each temperature point of a single condition was collected, pooled and centrifuged at maximum speed for 2 hours. The soluble fraction was collected for sample preparation for proteomic analysis.

Mass spectrometry data analysis for multiplexed quantitative proteomics

Peptides were separated prior to MS/MS analysis using an Easy-nLC (Thermo) equipped with an in-house pulled fused silica capillary column with integrated emitter packed with Accucore C18 media

(Thermo). Mass spectrometric analysis was carried out on an Orbitrap Eclipse (Thermo). For whole proteome profiling, separation was carried out with 90-minute gradients from 98% Buffer A (5% ACN, 0.125% formic acid) to 28% Buffer B (90% ACN, 0.125% formic acid). Multiplexed analysis of samples was done using real-time search data acquisition (Schweppe et al., 2020), based on canonical SPS-MS3 acquisition. Briefly, a survey MS1 scan was used to identify potential peptide precursors (R = 120000, Mass range: 400-2000 m/z, max Inject time: 50ms, AGC: 200%, RF lens: 30%). The top 10 precursors were selected for fragmentation and analysis in the ion trap (Dynamic exclusion: 90s at 10 ppm, CID collision energy: 35%, max inject time: 50 ms, AGC: 200%, scan rate: rapid, isolation width: 0.5 m/z). Real-time spectral matching was carried out using the Comet search algorithm (Eng et al., 2013). If, and only if, a peptide was matched with high confidence, the instrument would then acquire an additional SPS-MS3 scan for quantification of relative abundances (R = 50000, HCD NCE: 45, max injection time: 150 ms).

For phosphopeptide profiling, separation was carried out with 90-minute gradients from 98% Buffer A (5% ACN, 0.125% formic acid) to 26% Buffer B (90% ACN, 0.125% formic acid). Multiplexed analysis of samples was done using canonical SPS-MS3 acquisition. Briefly, a survey MS1 scan was used to identify potential peptide precursors (R = 120000, Mass range: 300-2000 m/z, max Inject time: 50ms, AGC: 200%, RF lens: 30%). The top 10 precursors were selected for fragmentation and analysis in the ion trap (Dynamic exclusion: 90s at 10 ppm, HCD NCE: 30, max inject time: 35 ms, AGC: 250%, scan rate: rapid, isolation width: 0.5 m/z). SPS-MS3 was carried out in the Orbitrap (R = 50000, AGC: 250%, HCD NCE: 45, max injection time: 86 ms).

Raw spectral information was converted to mzXML format using Monocle (Rad et al., 2021), and spectra were matched using the Comet search algorithm compared against the Uniprot human database. TMTpro is a static modification at the N-terminus of peptides. The maximum missed cleavage was set as 2. Peptides and proteins were filtered to a 1% using rules of protein parsimony.

Histone extraction and LC-MS/MS analysis for HDACi treatment

The histones were extracted and prepared for chemical derivatization and digestion as described previously (Bhanu et al., 2020; Sidoli et al., 2016). Briefly, lysine residues on histones were derivatized with the propionylation reagent (1:2 reagent:sample ratio) containing acetonitrile and propionic anhydride (3:1), with the solution pH adjusted to 8.0 using ammonium hydroxide. This propionylation reaction was performed twice and the samples were then dried using a speed vac. The derivatized histones were subsequently digested with trypsin at a 1:50 ratio (wt/wt) in 50 mM ammonium bicarbonate buffer at room temperature overnight. The N-termini of histone peptides were derivatized with the propionylation reagent twice and dried on speed vac (Searfoss et al., 2023). The peptides were desalted with the self-packed C18 stage tip. After desalting, the purified peptides were dried and reconstituted in 0.1% formic acid. Peptide analysis was performed using a LC-MS/MS system consisting of a Vanquish Neo UHPLC coupled to an Orbitrap Exploris 240 (Thermo Scientific). The histone peptide samples were kept at 7 °C on sample trays during LC analysis. Separation of peptides was carried out on an Easy-Spray™ PepMap™ Neo nano-column (2 µm, C18, 75 µm X 150 mm) at room temperature with a mobile phase. The chromatography conditions consisted of a linear gradient from 2 to 32% solvent B (0.1% formic acid in 100% acetonitrile) in solvent A (0.1% formic acid in water) over 48 minutes, followed by 42 to 98% solvent B over 12 minutes, at a flow rate of 300 nL/min. The mass spectrometer was programmed for data-independent acquisition (DIA) where each acquisition cycle consisted of a full MS scan, 35 DIA MS/MS scans of 24 m/z isolation width starting from 295 m/z to reach 1100 m/z. Typically, full MS scans were acquired in the Orbitrap mass analyzer across 290–1100 m/z at a resolution of 60,000 in positive profile mode with an auto maximum injection time and an AGC target of 300%. MS/MS data from HCD fragmentation was collected in the Orbitrap. These scans typically used an NCE of 30, an

AGC target of 1000%, and a maximum injection time of 60 ms. Histone MS data were analyzed with EpiProfile 2.0 (Z.-F. Yuan et al., 2015) .

Transcriptomics

Data regarding the HDACi-induced transcriptomic response in A549 was obtained from the NCBI GEO database under sample GSM4150378 (Srivatsan et al., 2020). Briefly, in this study, A549, MCF7, and K562 cells were treated with 4 increasing doses of a library of 188 small molecule compounds, including a subset of HDACi. The treated cells were subjected to high-throughput combinatorial indexing single-cell RNA-seq (sci-RNA-seq3). For this analysis, R package *monocle3* was used to analyze differentially expressed genes (DEGs) and for UMAP visualization (Trapnell et al., 2014; Qiu et al., 2017; J. Cao et al., 2019). For DEG analysis, the *celldataset* (cds) object was filtered to contain only A549 cells exposed to HDACi or vehicle control. For each HDACi, a generalized linear model was used to fit gene expression as a function of dose and replicate (quasi-Poisson regression) using *monocle3*'s *fit_models* function. This operation was performed on 7832 genes, determined as the union of genes expressed in 5% of cells per each inhibitor group. The p-values (Wald test) were FDR-corrected using the Benjamini-Hochberg method for multiple hypotheses, and the beta coefficients related to the contribution of dose were extracted and filtered as normalized beta coefficient > 0.05 and FDR < 5% for downstream comparison. Lastly, we performed batch integration (Haghverdi et al., 2018) and dimensional reduction (McInnes et al., 2018) of A549 cells treated with Abexinostat, Belinostat, Panobinostat, Trichostatin A, or vehicle to visualize cellular responses to HDACi.

Data analysis

Protein quantification tables containing normalized TMT abundance ratios were analyzed with python. Coefficient of variation (CV) between replicates was calculated and filtered (CV < 0.3) before being calculated relative to DMSO. Networks were imported from BioPlex 3.0 (Schweppe et al., 2018; Huttlin et al., 2021) and modified in Cytoscape (Shannon et al., 2003). Molecular docking of belinostat (PubChem: 6918638) to AURKB (PDB: 4AF3 (Elkins et al., 2012)) was performed using AutoDock 4.2 within AutoDockTools 1.5.7 (Morris et al., 2009). Docking was performed using 100 Genetic Algorithm runs with Lamarckian output, all other parameters were set to default parameters.

Software used as listed:

Software	**Version**
Python	3.11.1
pandas	2.1.4
numpy	1.26.3
matplotlib	3.7.0
plotnine	0.12.4
scipy	1.11.3
statsmodels	0.14.0
PyComplexHeatmap	1.6.1

seaborn	0.13.0
gsepy	1.1.1
scikit-learn	1.3.1
Cytoscape	3.10.1
BioPlex	3.0
AutoDockTools	1.5.7
AutoDock	4.2

Data availability

For total proteomics and phosphoproteomics, 70 .RAW files have been deposited to the ProteomeXchange Consortium via the PRIDE partner repository with the data set identifier PXD051206 (Username: reviewer_pxd051206@ebi.ac.uk, password: DyNpQWlR). Spectra were searched against the human Uniprot database (download v.05/2020).

Acknowledgement

We would like to acknowledge our funding sources: R35GM150919-01 (DKS), an Andy Hill CARE Distinguished Researcher Award (DKS), and a Cancer Consortium New Investigator Award (DKS). Support for this project was also provided by The Pew Charitable Trusts (DKS).

Conflict of Interest:

We acknowledge our ongoing collaborations and sponsored agreements with Thermo Fisher Scientific, Genentech, and AI Proteins.

Author contributions

C.L. and D.K.S. conceptualized the study. B.G., J.M. and D.K.S. supervised the experiments. C.L., C.S.,C.M.,R.K. and R.G. performed experiments. C.L. analyzed the data. C.L. drafted the original manuscript. Everyone reviewed and edited the manuscript. D.K.S. acquired funding.

Reference

Adhikary, S., Sanyal, S., Basu, M., Sengupta, I., Sen, S., Srivastava, D. K., Roy, S., & Das, C. (2016). Selective Recognition of H3.1K36 Dimethylation/H4K16 Acetylation Facilitates the Regulation of All-trans-retinoic Acid (ATRA)-responsive Genes by Putative Chromatin Reader ZMYND8. *The Journal of Biological Chemistry*, *291*(6), 2664–2681. https://doi.org/10.1074/jbc.M115.679985

Alvarez, F., Muñoz, F., Schilcher, P., Imhof, A., Almouzni, G., & Loyola, A. (2011). Sequential

Establishment of Marks on Soluble Histones H3 and H4. *The Journal of Biological Chemistry*, *286*(20), 17714–17721. https://doi.org/10.1074/jbc.M111.223453

Begley, C. G., & Ellis, L. M. (2012). Raise standards for preclinical cancer research. *Nature*, *483*(7391), 531–533. https://doi.org/10.1038/483531a

Bhanu, N. V., Sidoli, S., & Garcia, B. A. (2020). A Workflow for Ultra-rapid Analysis of Histone Post-translational Modifications with Direct-injection Mass Spectrometry. *Bio-Protocol*, *10*(18), e3756. https://doi.org/10.21769/BioProtoc.3756

Blackledge, N. P., & Klose, R. J. (2021). The molecular principles of gene regulation by Polycomb repressive complexes. *Nature Reviews. Molecular Cell Biology*, *22*(12), 815–833. https://doi.org/10.1038/s41580-021-00398-y

Bockstaele, L., Kooken, H., Libert, F., Paternot, S., Dumont, J. E., de Launoit, Y., Roger, P. P., & Coulonval, K. (2006). Regulated Activating Thr172 Phosphorylation of Cyclin-Dependent Kinase 4(CDK4): Its Relationship with Cyclins and CDK "Inhibitors." *Molecular and Cellular Biology*, *26*(13), 5070–5085. https://doi.org/10.1128/MCB.02006-05

Buggy, J. J., Cao, Z. A., Bass, K. E., Verner, E., Balasubramanian, S., Liu, L., Schultz, B. E., Young, P. R., & Dalrymple, S. A. (2006). CRA-024781: A novel synthetic inhibitor of histone deacetylase enzymes with antitumor activity in vitro and in vivo. *Molecular Cancer Therapeutics*, *5*(5), 1309–1317. https://doi.org/10.1158/1535-7163.MCT-05-0442

Cao, J., Spielmann, M., Qiu, X., Huang, X., Ibrahim, D. M., Hill, A. J., Zhang, F., Mundlos, S., Christiansen, L., Steemers, F. J., Trapnell, C., & Shendure, J. (2019). The single-cell transcriptional landscape of mammalian organogenesis. *Nature*, *566*(7745), 496–502. https://doi.org/10.1038/s41586-019-0969-x

Cao, X. X., Mohuiddin, I., Ece, F., McConkey, D. J., & Smythe, W. R. (2001). Histone Deacetylase Inhibitor Downregulation of bcl-xl Gene Expression Leads to Apoptotic Cell Death in Mesothelioma. *American Journal of Respiratory Cell and Molecular Biology*, *25*(5), 562–568. https://doi.org/10.1165/ajrcmb.25.5.4539

Caslini, C., Hong, S., Ban, Y. J., Chen, X. S., & Ince, T. A. (2019). HDAC7 regulates histone 3 lysine 27 acetylation and transcriptional activity at super-enhancer-associated genes in breast cancer stem cells. *Oncogene*, *38*(39), 6599–6614. https://doi.org/10.1038/s41388-019-0897-0

Chen, P.-H., Cai, L., Huffman, K., Yang, C., Kim, J., Faubert, B., Boroughs, L., Ko, B., Sudderth, J., McMillan, E. A., Girard, L., Chen, D., Peyton, M., Shields, M. D., Yao, B., Shames, D. S., Kim, H. S., Timmons, B., Sekine, I., … DeBerardinis, R. J. (2019). Metabolic Diversity in Human Non-Small Cell Lung Cancer Cells. *Molecular Cell*, *76*(5), 838-851.e5. https://doi.org/10.1016/j.molcel.2019.08.028

Chen, S., Yang, Z., Wilkinson, A. W., Deshpande, A. J., Sidoli, S., Krajewski, K., Strahl, B. D., Garcia, B. A., Armstrong, S. A., Patel, D. J., & Gozani, O. (2015). The PZP Domain of AF10 Senses Unmodified H3K27 to Regulate DOT1L-Mediated Methylation of H3K79. *Molecular Cell*, *60*(2), 319–327. https://doi.org/10.1016/j.molcel.2015.08.019

Cong, P., Jie, Z., Ying, L. H., Ming, Z., Li, W. L., Hong, Z. Q., Xin, Y. Y., Wei, X., Rong, S. S., Ling, L. X., & Yuan, L. G. (2006). The transcriptional regulation role of BRD7 by binding to acetylated histone through bromodomain. *Journal of Cellular Biochemistry*, *97*(4), 882–892. https://doi.org/10.1002/jcb.20645

Corpet, A., De Koning, L., Toedling, J., Savignoni, A., Berger, F., Lemaître, C., O'Sullivan, R. J., Karlseder, J., Barillot, E., Asselain, B., Sastre□Garau, X., & Almouzni, G. (2011). Asf1b, the necessary Asf1 isoform for proliferation, is predictive of outcome in breast cancer. *The EMBO Journal*, *30*(3), 480–493. https://doi.org/10.1038/emboj.2010.335

Corsello, S. M., Nagari, R. T., Spangler, R. D., Rossen, J., Kocak, M., Bryan, J. G., Humeidi, R., Peck, D., Wu, X., Tang, A. A., Wang, V. M., Bender, S. A., Lemire, E., Narayan, R., Montgomery, P., Ben-David, U., Garvie, C. W., Chen, Y., Rees, M. G., … Golub, T. R. (2020). Discovering the anticancer potential of non-oncology drugs by systematic viability profiling. *Nature Cancer*, *1*(2), Article 2. https://doi.org/10.1038/s43018-019-0018-6

Datta, S. R., Katsov, A., Hu, L., Petros, A., Fesik, S. W., Yaffe, M. B., & Greenberg, M. E. (2000). 14-3-

3 Proteins and Survival Kinases Cooperate to Inactivate BAD by BH3 Domain Phosphorylation. *Molecular Cell*, *6*(1), 41–51. https://doi.org/10.1016/S1097-2765(05)00012-2

Ding, C., Tang, W., Wu, H., Fan, X., Luo, J., Feng, J., Wen, K., & Wu, G. (2019). The PEAK1–PPP1R12B axis inhibits tumor growth and metastasis by regulating Grb2/PI3K/Akt signalling in colorectal cancer. *Cancer Letters*, *442*, 383–395. https://doi.org/10.1016/j.canlet.2018.11.014

Eckert, S., Berner, N., Kramer, K., Schneider, A., Müller, J., Lechner, S., Brajkovic, S., Sakhteman, A., Graetz, C., Fackler, J., Dudek, M., Pfaffl, M. W., Knolle, P., Wilhelm, S., & Kuster, B. (2024). Decrypting the molecular basis of cellular drug phenotypes by dose-resolved expression proteomics. *Nature Biotechnology*, 1–10. https://doi.org/10.1038/s41587-024-02218-y

Elkins, J. M., Santaguida, S., Musacchio, A., & Knapp, S. (2012). Crystal structure of human aurora B in complex with INCENP and VX-680. *Journal of Medicinal Chemistry*, *55*(17), 7841–7848. https://doi.org/10.1021/jm3008954

Eng, J. K., Jahan, T. A., & Hoopmann, M. R. (2013). Comet: An open-source MS/MS sequence database search tool. *PROTEOMICS*, *13*(1), 22–24. https://doi.org/10.1002/pmic.201200439

Fandy, T. E., & Srivastava, R. K. (2006). Trichostatin A sensitizes TRAIL-resistant myeloma cells by downregulation of the antiapoptotic Bcl-2 proteins. *Cancer Chemotherapy and Pharmacology*, *58*(4), 471–477. https://doi.org/10.1007/s00280-005-0184-3

Gaetani, M., Sabatier, P., Saei, A. A., Beusch, C. M., Yang, Z., Lundström, S. L., & Zubarev, R. A. (2019). Proteome Integral Solubility Alteration: A High-Throughput Proteomics Assay for Target Deconvolution. *Journal of Proteome Research*, *18*(11), 4027–4037. https://doi.org/10.1021/acs.jproteome.9b00500

Gajewski, T. F., & Thompson, C. B. (1996). Apoptosis Meets Signal Transduction: Elimination of a BAD Influence. *Cell*, *87*(4), 589–592. https://doi.org/10.1016/S0092-8674(00)81377-X

Ghandi, M., Huang, F. W., Jané-Valbuena, J., Kryukov, G. V., Lo, C. C., McDonald, E. R., Barretina, J., Gelfand, E. T., Bielski, C. M., Li, H., Hu, K., Andreev-Drakhlin, A. Y., Kim, J., Hess, J. M., Haas, B. J., Aguet, F., Weir, B. A., Rothberg, M. V., Paolella, B. R., … Sellers, W. R. (2019).

Next-generation characterization of the Cancer Cell Line Encyclopedia. *Nature*, *569*(7757), 503–508. https://doi.org/10.1038/s41586-019-1186-3

Haghverdi, L., Lun, A. T. L., Morgan, M. D., & Marioni, J. C. (2018). Batch effects in single-cell RNA sequencing data are corrected by matching mutual nearest neighbours. *Nature Biotechnology*, *36*(5), 421–427. https://doi.org/10.1038/nbt.4091

Hakimi, M.-A., Dong, Y., Lane, W. S., Speicher, D. W., & Shiekhattar, R. (2003). A Candidate X-linked Mental Retardation Gene Is a Component of a New Family of Histone Deacetylase-containing Complexes *. *Journal of Biological Chemistry*, *278*(9), 7234–7239. https://doi.org/10.1074/jbc.M208992200

Hirsch, C. L., Smith-Windsor, E. L., & Bonham, K. (2006). Src family kinase members have a common response to histone deacetylase inhibitors in human colon cancer cells. *International Journal of Cancer*, *118*(3), 547–554. https://doi.org/10.1002/ijc.21383

Hu, J., & Colburn, N. H. (2005). Histone deacetylase inhibition down-regulates cyclin D1 transcription by inhibiting nuclear factor-kappaB/p65 DNA binding. *Molecular Cancer Research: MCR*, *3*(2), 100–109. https://doi.org/10.1158/1541-7786.MCR-04-0070

Hu, K., Wu, W., Li, Y., Lin, L., Chen, D., Yan, H., Xiao, X., Chen, H., Chen, Z., Zhang, Y., Xu, S., Guo, Y., Koeffler, H. P., Song, E., & Yin, D. (2019). Poly(ADP-ribosyl)ation of BRD7 by PARP1 confers resistance to DNA-damaging chemotherapeutic agents. *EMBO Reports*, *20*(5), e46166. https://doi.org/10.15252/embr.201846166

Huttlin, E. L., Bruckner, R. J., Navarrete-Perea, J., Cannon, J. R., Baltier, K., Gebreab, F., Gygi, M. P., Thornock, A., Zarraga, G., Tam, S., Szpyt, J., Gassaway, B. M., Panov, A., Parzen, H., Fu, S., Golbazi, A., Maenpaa, E., Stricker, K., Guha Thakurta, S., … Gygi, S. P. (2021). Dual proteome-scale networks reveal cell-specific remodeling of the human interactome. *Cell*, *184*(11), 3022-3040.e28. https://doi.org/10.1016/j.cell.2021.04.011

Jasencakova, Z., Scharf, A. N. D., Ask, K., Corpet, A., Imhof, A., Almouzni, G., & Groth, A. (2010). Replication Stress Interferes with Histone Recycling and Predeposition Marking of New

Histones. *Molecular Cell*, *37*(5), 736–743. https://doi.org/10.1016/j.molcel.2010.01.033

Jiang, X., Tan, J., Li, J., Kivimäe, S., Yang, X., Zhuang, L., Lee, P. L., Chan, M. T. W., Stanton, L. W., Liu, E. T., Cheyette, B. N. R., & Yu, Q. (2008). DACT3 is an epigenetic regulator of Wnt/beta-catenin signaling in colorectal cancer and is a therapeutic target of histone modifications. *Cancer Cell*, *13*(6), 529–541. https://doi.org/10.1016/j.ccr.2008.04.019

Joseph, C., Al-Izzi, S., Alsaleem, M., Kurozumi, S., Toss, M. S., Arshad, M., Goh, F. Q., Alshankyty, I. M., Aleskandarany, M. A., Ali, S., Ellis, I. O., Mongan, N. P., Green, A. R., & Rakha, E. A. (2019). Retinoid X receptor gamma (RXRG) is an independent prognostic biomarker in ER-positive invasive breast cancer. *British Journal of Cancer*, *121*(9), 776–785. https://doi.org/10.1038/s41416-019-0589-0

LaBaer, J., Garrett, M. D., Stevenson, L. F., Slingerland, J. M., Sandhu, C., Chou, H. S., Fattaey, A., & Harlow, E. (1997). New functional activities for the p21 family of CDK inhibitors. *Genes & Development*, *11*(7), 847–862. https://doi.org/10.1101/gad.11.7.847

Lechner, S., Malgapo, M. I. P., Grätz, C., Steimbach, R. R., Baron, A., Rüther, P., Nadal, S., Stumpf, C., Loos, C., Ku, X., Prokofeva, P., Lautenbacher, L., Heimburg, T., Würf, V., Meng, C., Wilhelm, M., Sippl, W., Kleigrewe, K., Pauling, J. K., … Médard, G. (2022). Target deconvolution of HDAC pharmacopoeia reveals MBLAC2 as common off-target. *Nature Chemical Biology*, *18*(8), 812–820. https://doi.org/10.1038/s41589-022-01015-5

Leon, C., Manley, E., Neely, A. M., Castillo, J., Ramos Correa, M., Velarde, D. A., Yang, M., Puente, P. E., Romero, D. I., Ren, B., Chai, W., Gladstone, M., Lamango, N. S., Huang, Y., & Offringa, I. A. (2023). Lack of racial and ethnic diversity in lung cancer cell lines contributes to lung cancer health disparities. *Frontiers in Oncology*, *13*. https://www.frontiersin.org/articles/10.3389/fonc.2023.1187585

Leung, J. W. C., Makharashvili, N., Agarwal, P., Chiu, L.-Y., Pourpre, R., Cammarata, M. B., Cannon, J. R., Sherker, A., Durocher, D., Brodbelt, J. S., Paull, T. T., & Miller, K. M. (2017). ZMYM3 regulates BRCA1 localization at damaged chromatin to promote DNA repair. *Genes &*

Development, *31*(3), 260–274. https://doi.org/10.1101/gad.292516.116

Leutert, M., Rodríguez□Mias, R. A., Fukuda, N. K., & Villén, J. (2019). R2□P2 rapid□robotic phosphoproteomics enables multidimensional cell signaling studies. *Molecular Systems Biology*, *15*(12), e9021. https://doi.org/10.15252/msb.20199021

Li, N., Li, Y., Lv, J., Zheng, X., Wen, H., Shen, H., Zhu, G., Chen, T.-Y., Dhar, S. S., Kan, P.-Y., Wang, Z., Shiekhattar, R., Shi, X., Lan, F., Chen, K., Li, W., Li, H., & Lee, M. G. (2016). ZMYND8 reads the dual histone mark H3K4me1-H3K14ac to antagonize the expression of metastasis-linked genes. *Molecular Cell*, *63*(3), 470–484. https://doi.org/10.1016/j.molcel.2016.06.035

Li, X., Song, S., Liu, Y., Ko, S.-H., & Kao, H.-Y. (2004). Phosphorylation of the Histone Deacetylase 7 Modulates Its Stability and Association with 14-3-3 Proteins *. *Journal of Biological Chemistry*, *279*(33), 34201–34208. https://doi.org/10.1074/jbc.M405179200

Li, Y., & Seto, E. (2016). HDACs and HDAC Inhibitors in Cancer Development and Therapy. *Cold Spring Harbor Perspectives in Medicine*, *6*(10), a026831. https://doi.org/10.1101/cshperspect.a026831

Liberzon, A., Birger, C., Thorvaldsdóttir, H., Ghandi, M., Mesirov, J. P., & Tamayo, P. (2015). The Molecular Signatures Database (MSigDB) hallmark gene set collection. *Cell Systems*, *1*(6), 417–425. https://doi.org/10.1016/j.cels.2015.12.004

Lin, C., Song, W., Bi, X., Zhao, J., Huang, Z., Li, Z., Zhou, J., Cai, J., & Zhao, H. (2014). Recent advances in the ARID family: Focusing on roles in human cancer. *OncoTargets and Therapy*, *7*, 315–324. https://doi.org/10.2147/OTT.S57023

Liu, X., Song, J., Zhang, Y., Wang, H., Sun, H., Feng, X., Hou, M., Chen, G., Tang, Q., & Ji, M. (2020). ASF1B promotes cervical cancer progression through stabilization of CDK9. *Cell Death & Disease*, *11*(8), 1–15. https://doi.org/10.1038/s41419-020-02872-5

Liu, Y.-L., Yang, P.-M., Shun, C.-T., Wu, M.-S., Weng, J.-R., & Chen, C.-C. (2010). Autophagy potentiates the anti-cancer effects of the histone deacetylase inhibitors in hepatocellular carcinoma. *Autophagy*, *6*(8), 1057–1065. https://doi.org/10.4161/auto.6.8.13365

Lizcano, J. M., Morrice, N., & Cohen, P. (2000). Regulation of BAD by cAMP-dependent protein kinase is mediated via phosphorylation of a novel site, Ser155. *Biochemical Journal*, *349*(Pt 2), 547–557.

LoPiccolo, J., Gusev, A., Christiani, D. C., & Jänne, P. A. (2024). Lung cancer in patients who have never smoked—An emerging disease. *Nature Reviews Clinical Oncology*, *21*(2), 121–146. https://doi.org/10.1038/s41571-023-00844-0

Lowenstein, E. J., Daly, R. J., Batzer, A. G., Li, W., Margolis, B., Lammers, R., Ullrich, A., Skolnik, E. Y., Bar-Sagi, D., & Schlessinger, J. (1992). The SH2 and SH3 domain-containing protein GRB2 links receptor tyrosine kinases to ras signaling. *Cell*, *70*(3), 431–442. https://doi.org/10.1016/0092-8674(92)90167-b

Ma, C., & D'Mello, S. R. (2011). Neuroprotection by Histone Deacetylase-7 (HDAC7) Occurs by Inhibition of c-jun Expression through a Deacetylase-independent Mechanism. *The Journal of Biological Chemistry*, *286*(6), 4819–4828. https://doi.org/10.1074/jbc.M110.146860

Mader, M., de Dios, A., Shih, C., Bonjouklian, R., Li, T., White, W., López de Uralde, B., Sánchez-Martinez, C., del Prado, M., Jaramillo, C., de Diego, E., Martín Cabrejas, L. M., Dominguez, C., Montero, C., Shepherd, T., Dally, R., Toth, J. E., Chatterjee, A., Pleite, S., … Anderson, B. D. (2008). Imidazolyl benzimidazoles and imidazo[4,5-b]pyridines as potent p38alpha MAP kinase inhibitors with excellent in vivo antiinflammatory properties. *Bioorganic & Medicinal Chemistry Letters*, *18*(1), 179–183. https://doi.org/10.1016/j.bmcl.2007.10.106

Majumdar, G., Adris, P., Bhargava, N., Chen, H., & Raghow, R. (2012). Pan-histone deacetylase inhibitors regulate signaling pathways involved in proliferative and pro-inflammatory mechanisms in H9c2 cells. *BMC Genomics*, *13*(1), 709. https://doi.org/10.1186/1471-2164-13-709

Maltz, E., & Wollman, R. (2022). Quantifying the phenotypic information in mRNA abundance. *Molecular Systems Biology*, *18*(8), e11001. https://doi.org/10.15252/msb.202211001

Mamdani, H., & Jalal, S. I. (2020). Histone Deacetylase Inhibition in Non-small Cell Lung Cancer: Hype

or Hope? *Frontiers in Cell and Developmental Biology*, *8*. https://www.frontiersin.org/articles/10.3389/fcell.2020.582370

Mann, B. S., Johnson, J. R., Cohen, M. H., Justice, R., & Pazdur, R. (2007). FDA Approval Summary: Vorinostat for Treatment of Advanced Primary Cutaneous T-Cell Lymphoma. *The Oncologist*, *12*(10), 1247–1252. https://doi.org/10.1634/theoncologist.12-10-1247

Mann, J., Githaka, J. M., Buckland, T. W., Yang, N., Montpetit, R., Patel, N., Li, L., Baksh, S., Godbout, R., Lemieux, H., & Goping, I. S. (2019). Non-canonical BAD activity regulates breast cancer cell and tumor growth via 14-3-3 binding and mitochondrial metabolism. *Oncogene*, *38*(18), 3325–3339. https://doi.org/10.1038/s41388-018-0673-6

McDermott, J., & Jimeno, A. (2014). Belinostat for the treatment of peripheral T-cell lymphomas. *Drugs of Today (Barcelona, Spain*, *50*(5), 337–345. https://doi.org/10.1358/dot.2014.50.5.2138703

McInnes, L., Healy, J., Saul, N., & Großberger, L. (2018). UMAP: Uniform Manifold Approximation and Projection. *Journal of Open Source Software*, *3*(29), 861. https://doi.org/10.21105/joss.00861

Mitchell, D. C., Kuljanin, M., Li, J., Van Vranken, J. G., Bulloch, N., Schweppe, D. K., Huttlin, E. L., & Gygi, S. P. (2023). A proteome-wide atlas of drug mechanism of action. *Nature Biotechnology*. https://doi.org/10.1038/s41587-022-01539-0

Miyanaga, A., Gemma, A., Noro, R., Kataoka, K., Matsuda, K., Nara, M., Okano, T., Seike, M., Yoshimura, A., Kawakami, A., Uesaka, H., Nakae, H., & Kudoh, S. (2008). Antitumor activity of histone deacetylase inhibitors in non-small cell lung cancer cells: Development of a molecular predictive model. *Molecular Cancer Therapeutics*, *7*(7), 1923–1930. https://doi.org/10.1158/1535-7163.MCT-07-2140

Morris, G. M., Huey, R., Lindstrom, W., Sanner, M. F., Belew, R. K., Goodsell, D. S., & Olson, A. J. (2009). AutoDock4 and AutoDockTools4: Automated docking with selective receptor flexibility. *Journal of Computational Chemistry*, *30*(16), 2785–2791. https://doi.org/10.1002/jcc.21256

Mukherjee, S., Sen, S., Adhikary, S., Sengupta, A., Mandal, P., Dasgupta, D., Chakrabarti, P., Roy, S., & Das, C. (2020). A novel role of tumor suppressor ZMYND8 in inducing differentiation of breast

cancer cells through its dual-histone binding function. *Journal of Biosciences*, *45*(1), 2. https://doi.org/10.1007/s12038-019-9980-5

Nagai, Y., Miyazawa, H., Huqun, null, Tanaka, T., Udagawa, K., Kato, M., Fukuyama, S., Yokote, A., Kobayashi, K., Kanazawa, M., & Hagiwara, K. (2005). Genetic heterogeneity of the epidermal growth factor receptor in non-small cell lung cancer cell lines revealed by a rapid and sensitive detection system, the peptide nucleic acid-locked nucleic acid PCR clamp. *Cancer Research*, *65*(16), 7276–7282. https://doi.org/10.1158/0008-5472.CAN-05-0331

Navarrete-Perea, J., Yu, Q., Gygi, S. P., & Paulo, J. A. (2018). Streamlined Tandem Mass Tag (SL-TMT) Protocol: An Efficient Strategy for Quantitative (Phospho)proteome Profiling Using Tandem Mass Tag-Synchronous Precursor Selection-MS3. *Journal of Proteome Research*, *17*(6), 2226–2236. https://doi.org/10.1021/acs.jproteome.8b00217

Nichol, J. N., Dupéré-Richer, D., Ezponda, T., Licht, J. D., & Miller, W. H. (2016). Chapter Three - H3K27 Methylation: A Focal Point of Epigenetic Deregulation in Cancer. In K. D. Tew & P. B. Fisher (Eds.), *Advances in Cancer Research* (Vol. 131, pp. 59–95). Academic Press. https://doi.org/10.1016/bs.acr.2016.05.001

Nishino, T. G., Miyazaki, M., Hoshino, H., Miwa, Y., Horinouchi, S., & Yoshida, M. (2008). 14-3-3 regulates the nuclear import of class IIa histone deacetylases. *Biochemical and Biophysical Research Communications*, *377*(3), 852–856. https://doi.org/10.1016/j.bbrc.2008.10.079

Nukaga, S., Yasuda, H., Tsuchihara, K., Hamamoto, J., Masuzawa, K., Kawada, I., Naoki, K., Matsumoto, S., Mimaki, S., Ikemura, S., Goto, K., Betsuyaku, T., & Soejima, K. (2017). Amplification of EGFR Wild-Type Alleles in Non-Small Cell Lung Cancer Cells Confers Acquired Resistance to Mutation-Selective EGFR Tyrosine Kinase Inhibitors. *Cancer Research*, *77*(8), 2078–2089. https://doi.org/10.1158/0008-5472.CAN-16-2359

Nusinow, D. P., Szpyt, J., Ghandi, M., Rose, C. M., McDonald, E. R., Kalocsay, M., Jané-Valbuena, J., Gelfand, E., Schweppe, D. K., Jedrychowski, M., Golji, J., Porter, D. A., Rejtar, T., Wang, Y. K., Kryukov, G. V., Stegmeier, F., Erickson, B. K., Garraway, L. A., Sellers, W. R., & Gygi, S. P.

(2020). Quantitative Proteomics of the Cancer Cell Line Encyclopedia. *Cell*, *180*(2), 387-402.e16. https://doi.org/10.1016/j.cell.2019.12.023

Papavassiliou, A. G., & Musti, A. M. (2020). The Multifaceted Output of c-Jun Biological Activity: Focus at the Junction of CD8 T Cell Activation and Exhaustion. *Cells*, *9*(11), 2470. https://doi.org/10.3390/cells9112470

Piao, J., Chen, L., Quan, T., Li, L., Quan, C., Piao, Y., Jin, T., & Lin, Z. (2016). Superior efficacy of co-treatment with the dual PI3K/mTOR inhibitor BEZ235 and histone deacetylase inhibitor Trichostatin A against NSCLC. *Oncotarget*, *7*(37), 60169–60180. https://doi.org/10.18632/oncotarget.11109

Poll, B. G., Leo, K. T., Deshpande, V., Jayatissa, N., Pisitkun, T., Park, E., Yang, C.-R., Raghuram, V., & Knepper, M. A. (2024). A resource database for protein kinase substrate sequence-preference motifs based on large-scale mass spectrometry data. *Cell Communication and Signaling□: CCS*, *22*, 137. https://doi.org/10.1186/s12964-023-01436-2

Qiu, X., Mao, Q., Tang, Y., Wang, L., Chawla, R., Pliner, H. A., & Trapnell, C. (2017). Reversed graph embedding resolves complex single-cell trajectories. *Nature Methods*, *14*(10), 979–982. https://doi.org/10.1038/nmeth.4402

Rad, R., Li, J., Mintseris, J., O'Connell, J., Gygi, S. P., & Schweppe, D. K. (2021). Improved Monoisotopic Mass Estimation for Deeper Proteome Coverage. *Journal of Proteome Research*, *20*(1), 591–598. https://doi.org/10.1021/acs.jproteome.0c00563

Raghavan, S. (2022). How inclusive are cell lines in preclinical engineered cancer models? *Disease Models & Mechanisms*, *15*(5), dmm049520. https://doi.org/10.1242/dmm.049520

Reid, T., Valone, F., Lipera, W., Irwin, D., Paroly, W., Natale, R., Sreedharan, S., Keer, H., Lum, B., Scappaticci, F., & Bhatnagar, A. (2004). Phase II trial of the histone deacetylase inhibitor pivaloyloxymethyl butyrate (Pivanex, AN-9) in advanced non-small cell lung cancer. *Lung Cancer*, *45*(3), 381–386. https://doi.org/10.1016/j.lungcan.2004.03.002

Richardson, P. G., Laubach, J. P., Lonial, S., Moreau, P., Yoon, S.-S., Hungria, V. T., Dimopoulos, M.

A., Beksac, M., Alsina, M., & San-Miguel, J. F. (2015). Panobinostat: A novel pan-deacetylase inhibitor for the treatment of relapsed or relapsed and refractory multiple myeloma. *Expert Review of Anticancer Therapy*, *15*(7), 737–748. https://doi.org/10.1586/14737140.2015.1047770

Richon, V. M., Sandhoff, T. W., Rifkind, R. A., & Marks, P. A. (2000). Histone deacetylase inhibitor selectively induces p21WAF1 expression and gene-associated histone acetylation. *Proceedings of the National Academy of Sciences*, *97*(18), 10014–10019. https://doi.org/10.1073/pnas.180316197

Richon, V. M., Webb, Y., Merger, R., Sheppard, T., Jursic, B., Ngo, L., Civoli, F., Breslow, R., Rifkind, R. A., & Marks, P. A. (1996). Second generation hybrid polar compounds are potent inducers of transformed cell differentiation. *Proceedings of the National Academy of Sciences of the United States of America*, *93*(12), 5705–5708.

Roboti, P., & High, S. (2012). The oligosaccharyltransferase subunits OST48, DAD1 and KCP2 function as ubiquitous and selective modulators of mammalian N-glycosylation. *Journal of Cell Science*, *125*(14), 3474–3484. https://doi.org/10.1242/jcs.103952

Sawai, C. M., Freund, J., Oh, P., Ndiaye-Lobry, D., Bretz, J. C., Strikoudis, A., Genesca, L., Trimarchi, T., Kelliher, M. A., Clark, M., Soulier, J., Chen-Kiang, S., & Aifantis, I. (2012). Therapeutic Targeting of the Cyclin D3:CDK4/6 Complex in T Cell Leukemia. *Cancer Cell*, *22*(4), 452–465. https://doi.org/10.1016/j.ccr.2012.09.016

Schrump, D. S., Fischette, M. R., Nguyen, D. M., Zhao, M., Li, X., Kunst, T. F., Hancox, A., Hong, J. A., Chen, G. A., Kruchin, E., Wright, J. J., Rosing, D. R., Sparreboom, A., Figg, W. D., & Steinberg, S. M. (2008). Clinical and Molecular Responses in Lung Cancer Patients Receiving Romidepsin. *Clinical Cancer Research*, *14*(1), 188–198. https://doi.org/10.1158/1078-0432.CCR-07-0135

Schweppe, D. K., Eng, J. K., Yu, Q., Bailey, D., Rad, R., Navarrete-Perea, J., Huttlin, E. L., Erickson, B. K., Paulo, J. A., & Gygi, S. P. (2020). Full-Featured, Real-Time Database Searching Platform Enables Fast and Accurate Multiplexed Quantitative Proteomics. *Journal of Proteome Research*, *19*(5), 2026–2034. https://doi.org/10.1021/acs.jproteome.9b00860

Schweppe, D. K., Huttlin, E. L., Harper, J. W., & Gygi, S. P. (2018). BioPlex Display: An Interactive Suite for Large-Scale AP–MS Protein–Protein Interaction Data. *Journal of Proteome Research*, *17*(1), 722–726. https://doi.org/10.1021/acs.jproteome.7b00572

Searfoss, R. M., Karki, R., Lin, Z., Robison, F., & Garcia, B. A. (2023). An Optimized and High-Throughput Method for Histone Propionylation and Data-Independent Acquisition Analysis for the Identification and Quantification of Histone Post-translational Modifications. *Journal of the American Society for Mass Spectrometry*, *34*(11), 2508–2517. https://doi.org/10.1021/jasms.3c00223

Segal, D., Maier, S., Mastromarco, G. J., Qian, W. W., Nabeel-Shah, S., Lee, H., Moore, G., Lacoste, J., Larsen, B., Lin, Z.-Y., Selvabaskaran, A., Liu, K., Smibert, C., Zhang, Z., Greenblatt, J., Peng, J., Lee, H. O., Gingras, A.-C., & Taipale, M. (2023). A central chaperone-like role for 14-3-3 proteins in human cells. *Molecular Cell*, *83*(6), 974-993.e15. https://doi.org/10.1016/j.molcel.2023.02.018

Shakespear, M. R., Halili, M. A., Irvine, K. M., Fairlie, D. P., & Sweet, M. J. (2011). Histone deacetylases as regulators of inflammation and immunity. *Trends in Immunology*, *32*(7), 335–343. https://doi.org/10.1016/j.it.2011.04.001

Shanmugam, G., Rakshit, S., & Sarkar, K. (2022). HDAC inhibitors: Targets for tumor therapy, immune modulation and lung diseases. *Translational Oncology*, *16*, 101312. https://doi.org/10.1016/j.tranon.2021.101312

Shannon, P., Markiel, A., Ozier, O., Baliga, N. S., Wang, J. T., Ramage, D., Amin, N., Schwikowski, B., & Ideker, T. (2003). Cytoscape: A software environment for integrated models of biomolecular interaction networks. *Genome Research*, *13*(11), 2498–2504. https://doi.org/10.1101/gr.1239303

Shen, C., Liu, M., Xu, R., Wang, G., Li, J., Chen, P., Ma, W., Mwangi, J., Lu, Q., Duan, Z., Zhang, Z., Dahmani, F. Z., Mackeigan, D. T., Ni, H., & Lai, R. (2020). The 14-3-3ζ-c-Src-integrin-β3 complex is vital for platelet activation. *Blood*, *136*(8), 974–988. https://doi.org/10.1182/blood.2019002314

Shulak, L., Beljanski, V., Chiang, C., Dutta, S. M., Van Grevenynghe, J., Belgnaoui, S. M., Nguyên, T. L.-A., Di Lenardo, T., Semmes, O. J., Lin, R., & Hiscott, J. (2014). Histone Deacetylase Inhibitors Potentiate Vesicular Stomatitis Virus Oncolysis in Prostate Cancer Cells by Modulating NF-κB-Dependent Autophagy. *Journal of Virology*, *88*(5), 2927–2940. https://doi.org/10.1128/jvi.03406-13

Siavoshian, S., Segain, J.-P., Kornprobst, M., Bonnet, C., Cherbut, C., Galmiche, J.-P., & Blottière, H. M. (2000). Butyrate and trichostatin A effects on the proliferation/differentiation of human intestinal epithelial cells: Induction of cyclin D3 and p21 expression. *Gut*, *46*(4), 507–514. https://doi.org/10.1136/gut.46.4.507

Sidoli, S., Bhanu, N. V., Karch, K. R., Wang, X., & Garcia, B. A. (2016). Complete Workflow for Analysis of Histone Post-translational Modifications Using Bottom-up Mass Spectrometry: From Histone Extraction to Data Analysis. *Journal of Visualized Experiments: JoVE*, *111*, 54112. https://doi.org/10.3791/54112

Srivatsan, S. R., McFaline-Figueroa, J. L., Ramani, V., Saunders, L., Cao, J., Packer, J., Pliner, H. A., Jackson, D. L., Daza, R. M., Christiansen, L., Zhang, F., Steemers, F., Shendure, J., & Trapnell, C. (2020). Massively multiplex chemical transcriptomics at single-cell resolution. *Science*, *367*(6473), 45–51. https://doi.org/10.1126/science.aax6234

Sugimoto, A., Hozak, R. R., Nakashima, T., Nishimoto, T., & Rothman, J. H. (1995). Dad□1, an endogenous programmed cell death suppressor in Caenorhabditis elegans and vertebrates. *The EMBO Journal*, *14*(18), 4434–4441. https://doi.org/10.1002/j.1460-2075.1995.tb00122.x

Sugiyama, N., Imamura, H., & Ishihama, Y. (2019). Large-scale Discovery of Substrates of the Human Kinome. *Scientific Reports*, *9*(1), 10503. https://doi.org/10.1038/s41598-019-46385-4

Suliman, B. A., Xu, D., & Williams, B. R. (2012). HDACi: Molecular mechanisms and therapeutic implications in the innate immune system. *Immunology & Cell Biology*, *90*(1), 23–32. https://doi.org/10.1038/icb.2011.92

Tan, Y., Demeter, M. R., Ruan, H., & Comb, M. J. (2000). BAD Ser-155 Phosphorylation Regulates

BAD/Bcl-XL Interaction and Cell Survival*. *Journal of Biological Chemistry*, *275*(33), 25865–25869. https://doi.org/10.1074/jbc.M004199200

Trapnell, C., Cacchiarelli, D., Grimsby, J., Pokharel, P., Li, S., Morse, M., Lennon, N. J., Livak, K. J., Mikkelsen, T. S., & Rinn, J. L. (2014). The dynamics and regulators of cell fate decisions are revealed by pseudotemporal ordering of single cells. *Nature Biotechnology*, *32*(4), 381–386. https://doi.org/10.1038/nbt.2859

Traynor, A. M., Dubey, S., Eickhoff, J. C., Kolesar, J. M., Schell, K., Huie, M. S., Groteluschen, D. L., Marcotte, S. M., Hallahan, C. M., Weeks, H. R., Wilding, G., Espinoza-Delgado, I., & Schiller, J. H. (2009). Vorinostat (NSC# 701852) in Patients with Relapsed Non-small Cell Lung Cancer: A Wisconsin Oncology Network Phase II Study. *Journal of Thoracic Oncology*, *4*(4), 522–526. https://doi.org/10.1097/JTO.0b013e3181952478

Trinei, M., Lanfrancone, L., Campo, E., Pulford, K., Mason, D. Y., Pelicci, P.-G., & Falini, B. (2000). A New Variant Anaplastic Lymphoma Kinase (ALK)-Fusion Protein (ATIC-ALK) in a Case of ALK-positive Anaplastic Large Cell Lymphoma1. *Cancer Research*, *60*(4), 793–798.

Tsherniak, A., Vazquez, F., Montgomery, P. G., Weir, B. A., Kryukov, G., Cowley, G. S., Gill, S., Harrington, W. F., Pantel, S., Krill-Burger, J. M., Meyers, R. M., Ali, L., Goodale, A., Lee, Y., Jiang, G., Hsiao, J., Gerath, W. F. J., Howell, S., Merkel, E., … Hahn, W. C. (2017). Defining a Cancer Dependency Map. *Cell*, *170*(3), 564-576.e16. https://doi.org/10.1016/j.cell.2017.06.010

Uhlen, M., Zhang, C., Lee, S., Sjöstedt, E., Fagerberg, L., Bidkhori, G., Benfeitas, R., Arif, M., Liu, Z., Edfors, F., Sanli, K., Von Feilitzen, K., Oksvold, P., Lundberg, E., Hober, S., Nilsson, P., Mattsson, J., Schwenk, J. M., Brunnström, H., … Ponten, F. (2017). A pathology atlas of the human cancer transcriptome. *Science*, *357*(6352), eaan2507. https://doi.org/10.1126/science.aan2507

Van Vranken, J. G., Li, J., Mintseris, J., Gadzuk-Shea, M., Gygi, S. P., & Schweppe, D. K. (2024). Large-scale characterization of drug mechanism of action using proteome-wide thermal shift assays. *bioRxiv*, 2024.01.26.577428. https://doi.org/10.1101/2024.01.26.577428

van der Meer, D., Barthorpe, S., Yang, W., Lightfoot, H., Hall, C., Gilbert, J., Francies, H. E., & Garnett, M. J. (2019). Cell Model Passports—A hub for clinical, genetic and functional datasets of preclinical cancer models. *Nucleic Acids Research*, *47*(Database issue), D923–D929. https://doi.org/10.1093/nar/gky872

Vrana, J. A., Decker, R. H., Johnson, C. R., Wang, Z., Jarvis, W. D., Richon, V. M., Ehinger, M., Fisher, P. B., & Grant, S. (1999). Induction of apoptosis in U937 human leukemia cells by suberoylanilide hydroxamic acid (SAHA) proceeds through pathways that are regulated by Bcl-2/Bcl-XL, c-Jun, and p21CIP1, but independent of p53. *Oncogene*, *18*(50), Article 50. https://doi.org/10.1038/sj.onc.1203176

Wang, D., Eraslan, B., Wieland, T., Hallström, B., Hopf, T., Zolg, D. P., Zecha, J., Asplund, A., Li, L., Meng, C., Frejno, M., Schmidt, T., Schnatbaum, K., Wilhelm, M., Ponten, F., Uhlen, M., Gagneur, J., Hahne, H., & Kuster, B. (2019). A deep proteome and transcriptome abundance atlas of 29 healthy human tissues. *Molecular Systems Biology*, *15*(2), e8503. https://doi.org/10.15252/msb.20188503

Wang, L., Wu, Z., Xia, Y., Lu, X., Li, J., Fan, L., Qiao, C., Qiu, H., Gu, D., Xu, W., Li, J., & Jin, H. (2022). Single-cell profiling-guided combination therapy of c-Fos and histone deacetylase inhibitors in diffuse large B-cell lymphoma. *Clinical and Translational Medicine*, *12*(5), e798. https://doi.org/10.1002/ctm2.798

Wensheng, L., Bo, Z., Qiangsheng, H., Wenyan, X., Shunrong, J., Jin, X., Quanxing, N., Xianjun, Y., & Xiaowu, X. (2019). MBD1 promotes the malignant behavior of gallbladder cancer cells and induces chemotherapeutic resistance to gemcitabine. *Cancer Cell International*, *19*(1), 232. https://doi.org/10.1186/s12935-019-0948-1

Wu, D., Yan, Y., Wei, T., Ye, Z., Xiao, Y., Pan, Y., Orme, J. J., Wang, D., Wang, L., Ren, S., & Huang, H. (2021). An acetyl-histone vulnerability in PI3K/AKT inhibition-resistant cancers is targetable by both BET and HDAC inhibitors. *Cell Reports*, *34*(7). https://doi.org/10.1016/j.celrep.2021.108744

Wu, L., Wang, Y., Liu, Y., Yu, S., Xie, H., Shi, X., Qin, S., Ma, F., Tan, T. Z., Thiery, J. P., & Chen, L. (2014). A central role for TRPS1 in the control of cell cycle and cancer development. *Oncotarget*, *5*(17), 7677–7690.

Xiao, H., Hasegawa, T., & Isobe, K. (1999). Both Sp1 and Sp3 are responsible for p21waf1 promoter activity induced by histone deacetylase inhibitor in NIH3T3 cells. *Journal of Cellular Biochemistry*, *73*(3), 291–302. https://doi.org/10.1002/(SICI)1097-4644(19990601)73:3<291::AID-JCB1>3.0.CO;2-5

Xie, Y., Sahin, M., Sinha, S., Wang, Y., Nargund, A. M., Lyu, Y., Han, S., Dong, Y., Hsieh, J. J., Leslie, C. S., & Cheng, E. H. (2022). SETD2 loss perturbs the kidney cancer epigenetic landscape to promote metastasis and engenders actionable dependencies on histone chaperone complexes. *Nature Cancer*, *3*(2), 188–202. https://doi.org/10.1038/s43018-021-00316-3

Yang, Y., Yin, L., Zhu, M., Song, S., Sun, C., Han, X., Xu, Y., Zhao, Y., Qi, Y., Xu, L., & Peng, J.-Y. (2021). Protective effects of dioscin on vascular remodeling in pulmonary arterial hypertension via adjusting GRB2/ERK/PI3K-AKT signal. *Biomedicine & Pharmacotherapy*, *133*, 111056. https://doi.org/10.1016/j.biopha.2020.111056

Yoshida, M., Kijima, M., Akita, M., & Beppu, T. (1990). Potent and specific inhibition of mammalian histone deacetylase both in vivo and in vitro by trichostatin A. *The Journal of Biological Chemistry*, *265*(28), 17174–17179.

Yuan, W., Xu, M., Huang, C., Liu, N., Chen, S., & Zhu, B. (2011). H3K36 methylation antagonizes PRC2-mediated H3K27 methylation. *The Journal of Biological Chemistry*, *286*(10), 7983–7989. https://doi.org/10.1074/jbc.M110.194027

Yuan, Z.-F., Lin, S., Molden, R. C., Cao, X.-J., Bhanu, N. V., Wang, X., Sidoli, S., Liu, S., & Garcia, B. A. (2015). EpiProfile Quantifies Histone Peptides With Modifications by Extracting Retention Time and Intensity in High-resolution Mass Spectra*,. *Molecular & Cellular Proteomics*, *14*(6), 1696–1707. https://doi.org/10.1074/mcp.M114.046011

Zecha, J., Bayer, F. P., Wiechmann, S., Woortman, J., Berner, N., Müller, J., Schneider, A., Kramer, K.,

Abril-Gil, M., Hopf, T., Reichart, L., Chen, L., Hansen, F. M., Lechner, S., Samaras, P., Eckert, S., Lautenbacher, L., Reinecke, M., Hamood, F., … Kuster, B. (2023). Decrypting drug actions and protein modifications by dose- and time-resolved proteomics. *Science*. https://doi.org/10.1126/science.ade3925

Zhang, J., Kalyankrishna, S., Wislez, M., Thilaganathan, N., Saigal, B., Wei, W., Ma, L., Wistuba, I. I., Johnson, F. M., & Kurie, J. M. (2007). Src-Family Kinases Are Activated in Non-Small Cell Lung Cancer and Promote the Survival of Epidermal Growth Factor Receptor-Dependent Cell Lines. *The American Journal of Pathology*, *170*(1), 366–376. https://doi.org/10.2353/ajpath.2007.060706

Zhang, Y., Remillard, D., Onubogu, U., Karakyriakou, B., Asiaban, J. N., Ramos, A. R., Bowland, K., Bishop, T. R., Barta, P. A., Nance, S., Durbin, A. D., Ott, C. J., Janiszewska, M., Cravatt, B. F., & Erb, M. A. (2023). Collateral lethality between HDAC1 and HDAC2 exploits cancer-specific NuRD complex vulnerabilities. *Nature Structural & Molecular Biology*, *30*(8), 1160–1171. https://doi.org/10.1038/s41594-023-01041-4

Zhou, F., & Zhou, C. (2018). Lung cancer in never smokers—The East Asian experience. *Translational Lung Cancer Research*, *7*(4). https://doi.org/10.21037/tlcr.2018.05.14

Zhou, M., Liu, H., Xu, X., Zhou, H., Li, X., Peng, C., Shen, S., Xiong, W., Ma, J., Zeng, Z., Fang, S., Nie, X., Yang, Y., Zhou, J., Xiang, J., Cao, L., Peng, S., Li, S., & Li, G. (2006). Identification of nuclear localization signal that governs nuclear import of BRD7 and its essential roles in inhibiting cell cycle progression. *Journal of Cellular Biochemistry*, *98*(4), 920–930. https://doi.org/10.1002/jcb.20788

Zhou, Y.-L., Zheng, C., Chen, Y.-T., & Chen, X.-M. (2018). Underexpression of INPPL1 is associated with aggressive clinicopathologic characteristics in papillary thyroid carcinoma. *OncoTargets and Therapy*, *11*, 7725–7731. https://doi.org/10.2147/OTT.S185803